CHAPTER 4: STRUCTURE-FUNCTION ASSOCIATIONS BETWEEN ELASTIC FIBRES AND COLLAGEN

4.1 Introduction

As outlined in Chapter 1, bending and compression of the intervertebral disc within the confines of each motion segment are made possible by the circumferential and axial expansion of the lamellae; this expansion is facilitated by both the direct extension of the collagen fibre bundles and their tilting relative to the transverse plane. In circumferential expansion, direct extension of collagen fibre bundles (fibre strain, measured at the peripheral surface) as a total percentage of tissue deformation is relatively large (Shah *et al.*, 1978; Stokes, 1987). In contrast, with respect to the positive axial deformations associated with bending, the percentage contribution of collagen fibre strain to total deformation (increase in disc height) is relatively small, suggesting that collagen fibre reorientation plays a more dominant role (Pearcy and Tibrewal, 1984; Stokes, 1987). Analytical structure-function modelling has highlighted the relative importance of shear and normal interactions in determining the tensile mechanical response anulus fibrosus specimens, particularly in the axial direction (Guerin and Elliott, 2007), which is consistent with the idea that relative collagen fibre reorientation is the predominating deformation mechanism for this orientation.

The structural mechanism which enables the extension of the collagen fibre bundles along their principle load bearing axis is the straightening of the collagen fibre planar crimp; extension of the bundles beyond the straightening of this crimp is limited and leads to progressive localised structural failure (Pezowicz *et al.*, 2005). The structural mechanism which facilitates tilting is relative collagen fibre reorientation, or inter-fibre ‘sliding’(Bruehlmann *et al.*, 2004b). In circumferential tension, the tilt angle (the angle of the fibres to the transverse plane) decreases as fibres re-orient towards the

loading direction; in axial tension the opposite occurs (Klein and Hukins, 1982a; Klein and Hukins, 1982b; Bruehlmann *et al.*, 2004a; Guerin and Elliott, 2006).

Tensile deformation of lamellae could therefore be considered a two-stage process: on the initial application of load, the straightening of crimp occurs first, functioning perhaps more as a shock-absorbing mechanism to prevent sudden impact damage to the collagen fibres, similar to in tendons; larger-scale tensile deformation, particularly that which occurs axially in bending, then follows, facilitated by collagen fibre re-orientation. The question that arises from this two-stage mechanism of deformation is: in which of these two modes is the functional role of intralamellar elastic fibres most important – crimp extension or collagen fibre reorientation?

There are a number of factors which appear to discount the possibility that elastic fibres play a significant role maintaining collagen crimp under zero strain and re-estabilishing crimp following deformation. Firstly, in section 3.6.3, three-dimensional reconstructions of elastic fibre arrangements in the lamellar plane demonstrated that a number of fibres were observed to mimic the crimp pattern of the surrounding collagen. This is consistent with the observations of another recent study (Yu *et al.*, 2007). If fibres were to be maintaining crimp, it is reasonable to assume that they would initially be under tension and hence appear straight, but the observation described suggests collagen crimp must straighten before elastic fibres become mechanically viable. Secondly, collagen crimp is present in other tissues which contain no documented elastic fibres, such as Achilles tendon, suggesting it is an intrinsic property determined by collagen ultrastructure (Raspanti *et al.*, 2005; Franchi *et al.*, 2007). Finally, the relatively small strains along the collagen fibre axes attributable to uncrimping (Stokes, 1987; Pezowicz *et al.*, 2005) would seem to make

elastic fibres redundant in consideration of their high extensibility (Fung, 1981). Irrespective of these factors, there is currently no conclusive evidence that in the anulus fibrosus, where elastic fibres and collagen appear to be closely integrated, elastic fibres play no role in maintaining collagen crimp, and an experimental investigation is thus warranted.

With respect to the second of these possibilities – that elastic fibres limit and reverse relative fibre reorientation – it would be, by inference, necessary for them to provide cross-collagen fibre mechanical connectivity; indeed, a recent histological study investigating the distribution of both elastin and fibrillin-1 in the human anulus proposed elastic fibres as likely cross-connecting elements within the aligned collagen fibre matrix (Yu *et al.*, 2007).

Such cross-collagen fibre connectivity by elastic fibres may also be important in the context of radial deformations. As outlined in section 1.2.1.4.1, nuclear migration during bending subjects the anulus to tensile radial strains of up to 10 percent, depending on disc condition, region and bending modality (Tsantrizos *et al.*, 2005). Anulus deformation in response to such strains occurs by way of both transverse collagen bundle elongation and separation at lamellar interfaces (section 1.2.1.3, illustrated in Figure 1.5) (Pezowicz *et al.*, 2006a). Elastic fibres potentially provide important transverse mechanical integrity that limits this deformation and assists its reversal.

As described in Chapter 3, elastic fibres located at the interfaces between consecutive lamellae display greater structural complexity than those within lamellae, perhaps due to the fact that they integrate with collagen fibres with opposite preferential

orientations. In bending, compression and torsion, the ‘interlamellar angle’ between collagen fibres in consecutive lamellae varies as those fibres tilt in opposite directions. This change in interlamellar angle constitutes significant shear at the lamellar interface (Bruehlmann *et al.*, 2004b). The mechanical function of interlamellar elastic fibres may be similar to intralamellar elastic fibres, but conveyed at a higher level of the structrual hierarchy – i.e. between lamellae instead of between fibres.

In this chapter, two experimental studies are described. The first addresses the possibility that elastic fibres maintain collagen planar crimp. It was hypothesized that targeted removal of elastic fibres would not result in passive relaxation (straightening) of the crimp morphology, thus demonstrating that the role of elastic fibres in maintaining and re-establishing crimp is minimal. The second study addresses the possibility that elastic fibres provide cross-collagen fibre and cross-lamellar connectivity. It was hypothesized that tensile strains applied to anulus tissue radially, perpendicular to the plane containing the collagen fibres, would result in a loss of the structural isotropy of the intralamellar elastic fibres that was described in Chapter 3, and that this loss of isotropy would be specifically characterised by elastic fibre skewing, extension and contraction, consistent with the relative separation and realignment of adjacent collagen fibres they cross-connect. Additionally, it was hypothesized that elastic fibres at lamellar interfaces would maintain physical connections between those lamellae undergoing transverse separation, as evidence of cross-lamellar connectivity.

4.2 Scope

Following a statement of objectives and hypotheses, methods and results are presented separately for the two experimental studies, followed by a unifying discussion.

4.3 Objectives and Hypotheses

The objective in this chapter was to qualitatively examine the nature of the structure-function associations between elastic fibres and collagen in the anulus fibrosus with respect to the distinct mechanisms of collagen tensile deformation, both within collagen fibre bundles (intralamellar) and between collagen fibre bundles in consecutive lamellae (interlamellar).

The following null hypotheses were proposed:

- Targeted enzymatic degradation of elastic fibres does result in passive distension of collagen planar crimp.

- Intralamellar elastic fibre isotropy is not affected by uniaxial strains applied perpendicular to the plane containing the collagen fibres.

- Interlamellar elastic fibres do not maintain connections between consecutive anulus fibrosus lamellae undergoing transverse separation.

The first of these hypotheses is tested in section 4.4 and the other two are tested section 4.5.

4.4 Elastic Fibres and Collagen Crimp

4.4.1 Methods

Specimens from four intervertebral discs, aged 16, 28, 53 (L1-L2) and 57 (L3-L4) with grades of 1, 2, 3 and 3 respectively, obtained and graded using the protocol described in section 2.2, were used. With reference to Figure 4.1, a specimen bordering the anulus periphery and approximately 10mm wide and 3mm deep, was removed from the lateral side of each hemi-disc. The outermost lamellae were carefully removed using a scalpel in order to exclude the possible presence of any extraneous soft tissue such as ligament. Each specimen was then divided in two parts (Figure 4.1), with one half allocated to an elastic fibre degradation group, and the other half to a buffer only control group.

To degrade elastic fibres, specimens were subjected to enzymatic treatment in 1ml of 0.2M Tris-HCl buffer, pH 8.6, containing 3 units of purified porcine pancreatic elastase, 3mg of soybean trypsin inhibitor, and 10mM N-ethylmaleimide and 5mM benzamidine hydrochloride as protease inhibitors. This treatment was developed further to include biochemical validation for use in the biomechanical investigation described in Chapter 5. For this study, histological validation of elastic fibre degradation was considered adequate. Specimens in the control group were treated in the same buffer with the three inhibitors, but omitting the enzyme. Both treatments were carried out over 36 hours at 37°C.

Following treatments, specimens were washed in PBS, fixed overnight in 10% buffered formalin at 4°C, then routinely processed (TissueTek VIP5J-F2, Sakura Finetek, Tokyo, Japan) and paraffin embedded. Using a rotary microtome (Model

1521, Leica Microsystems, Wetzlar, Germany) 30 μm sections were cut from each specimen in the lamellar plane, parallel to the circumferential surface of the disc (this orientation is defined diagrammatically in Figure 3.2).

To confirm successful degradation of elastic fibres, one section from each specimen was cleared of paraffin, rehydrated and stained with resorcin-fuchsin using the protocol described in 3.5.2.2. The presence or absence of elastic fibres was assessed qualitatively under phase contrast at 100 times objective magnification, and comparisons were made between elastase treated and control specimens. To assess collagen crimp morphology, one section from each specimen was cleared of paraffin, rehydrated and stained with van Gieson using the protocol described in 3.5.2.1. The presence of collagen crimp (or lack there of) was then assessed qualitatively under cross-polarised light at objective magnifications ranging from 10 to 40 times, and comparisons were made between elastase treated and control specimens.

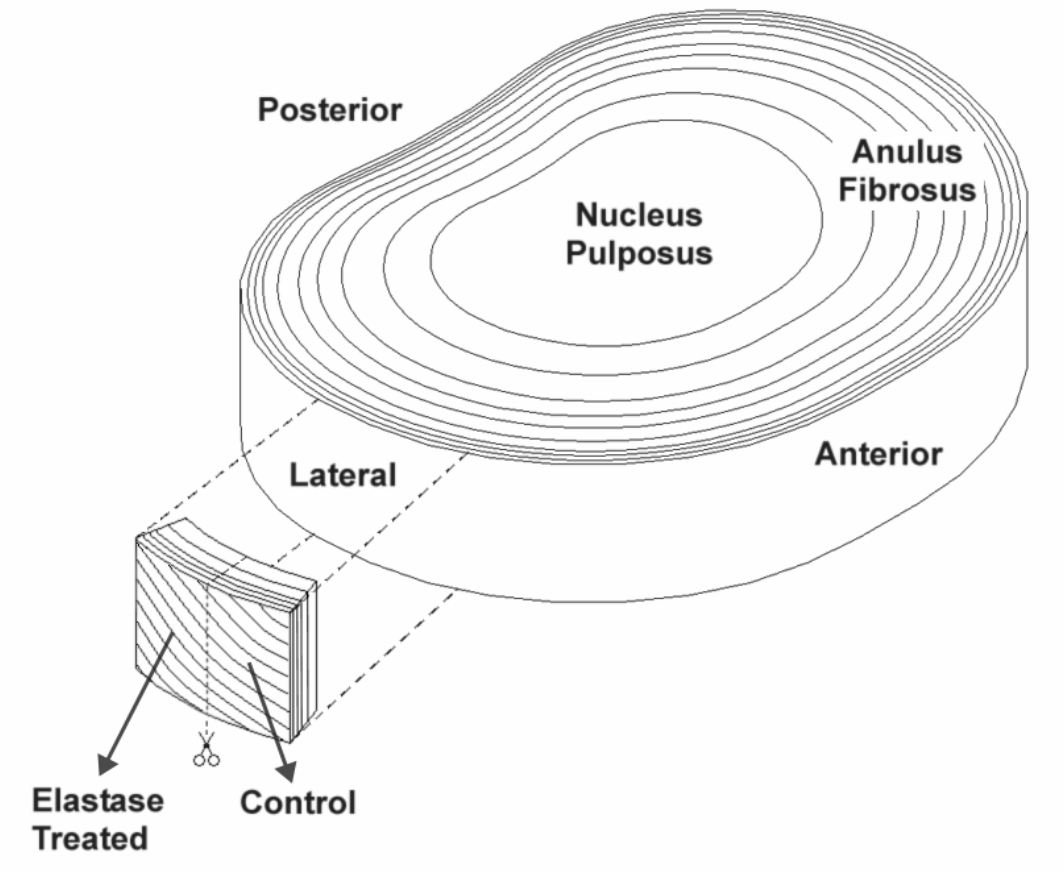


Figure 4.1. Schematic illustrating the excision site in the lateral anulus fibrosus for lamellar plane specimens used to investigate the role of elastic fibres in the maintaining collagen crimp.

4.4.2 Results

Assessment of sections stained with resorcin-fuchsin from each elastase-treated specimen revealed no elastic fibres, confirming that the degradation protocol was successful. In all control sections, intralamellar elastic fibres were abundant.

The images in Figure 4.2 show sections from elastase-treated and control specimens stained with van Gieson and viewed under cross-polarised light at 40 times objective magnification. Images on the left are those from controls and those on the right are those from elastase-treated specimens. Horizontally adjacent specimens reflect matched pairs corresponding to adjacent specimens taken from the same disc, as labelled. Collagen crimp appears consistently in all four specimens treated with elastase and appears morphologically similar to that observed in each respective control.

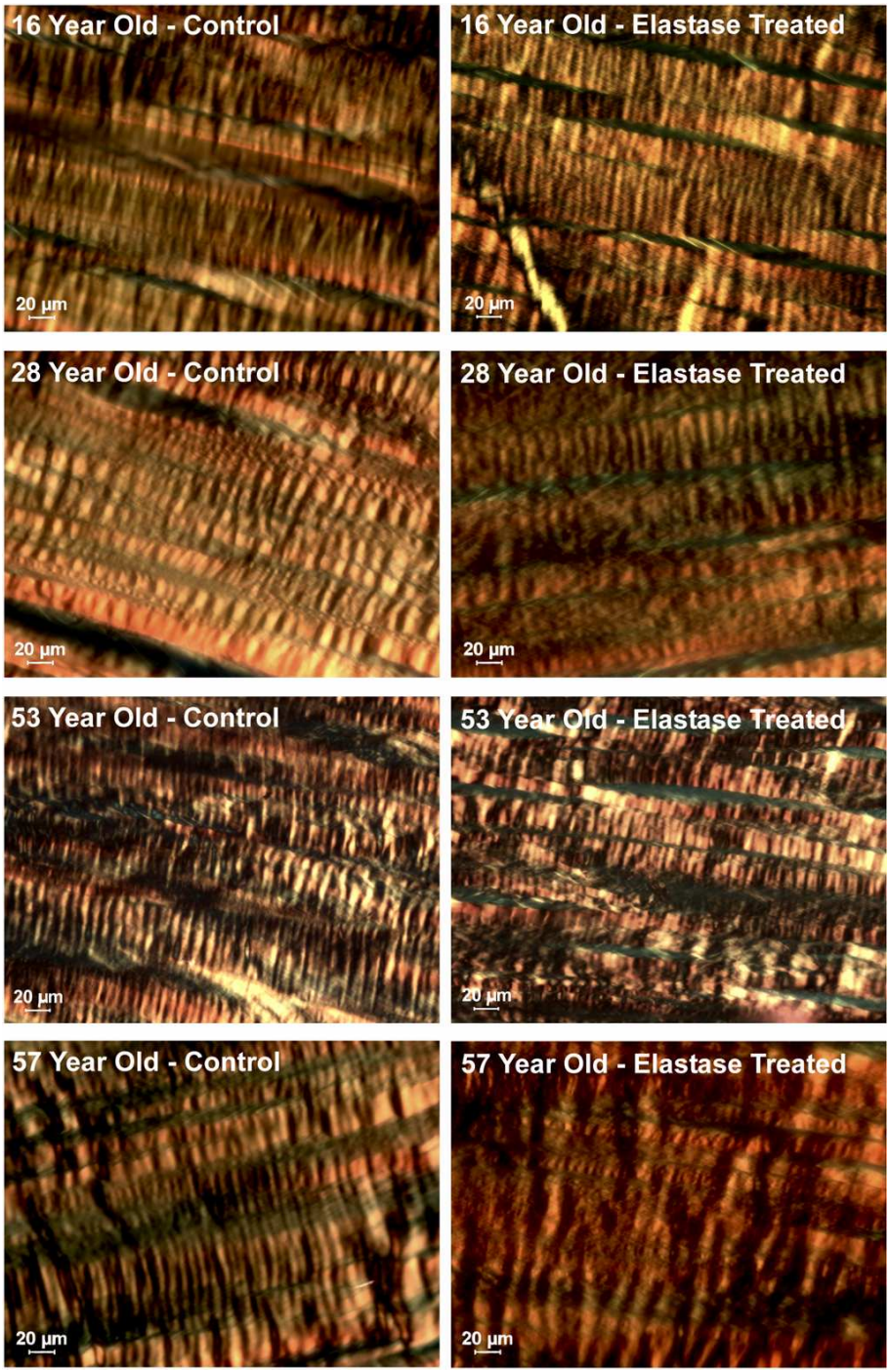


Figure 4.2. Crimp morphology in control and elastase treated specimens (30 micron lamellar plane sections, van Gieson stain, cross-polarised light, 40 times objective magnification).

4.5 Elastic Fibres and Cross-Collagen Fibre Connectivity

4.5.1 Methods

The posterolateral quadrants (Figure 4.3) from each of two L1-L2 discs, aged 40 and 60 with grades of 2 and 3 respectively were trimmed to a uniform thickness of approximately 2 mm on a cryostat (Miles Laboratories, Elkhart, Indiana USA), then a parallel-edged razor tool was used to cut to profile two 5 mm wide, radially oriented specimens, which were trimmed to an approximate length of 10 mm using a scalpel. This method of specimen preparation is comparable to that used for subsequent biomechanical experiments, and is described in further detail in section 5.4.2. Posterolateral quadrants were deliberately selected due to the higher elastic fibre density in this region (Figure 3.16).

One specimen from each disc was equilibrated in phosphate buffered saline and subjected to a uniaxial strain, the magnitude of which was less than the yield strain but in excess of the transition strain to the second linear region of the stress-strain response, as determined qualitatively in real time (mechanical testing system described in section 5.6.2.5), via a single ramp input at a rate of 50 microns per second. The location of the gauge region of each specimen corresponded approximately to the lamellae of the middle anulus. The specimen was clamped at the peak strain, then submerged immediately in ten percent buffered formalin and allowed to fix for 24 hours at 4°C. The specimen was then subjected to automated processing for 8 hours (TissueTek VIP5J-F2, Sakura Finetek, Tokyo, Japan) and paraffin embedded. Consecutive 30 μm sections were cut on a rotary microtome (Model 1521, Leica Microsystems, Wetzlar, Germany), mounted on gelatin-coated microscope

slides and stained with resorcin-fuchsin to demonstrate elastic fibres using the methodology described in section 3.5.2.2. The second specimen from each disc was equilibrated in saline then fixed in formalin without first being subjected to uniaxial strain in the manner described, to serve as a control, enabling histological comparisons to be made between adjacent strained and unstrained specimens.

Within the gauge region of each strained specimen, and in similar corresponding regions in respective control specimens, elastic fibres were visualised at objective magnifications up to 100 times under phase contrast, using the composite z-stack imaging technique, and post-processed in Matlab using the techniques outlined in section 3.5.3 as required. Elastic fibre architecture was studied both within collagen bundles and at lamellar interfaces, as illustrated schematically in Figure 4.3B.

Adjacent sections from both strained and control sections were stained with van Gieson to demonstrate general collagenous architecture, using the protocol described in section 3.5.2.1.

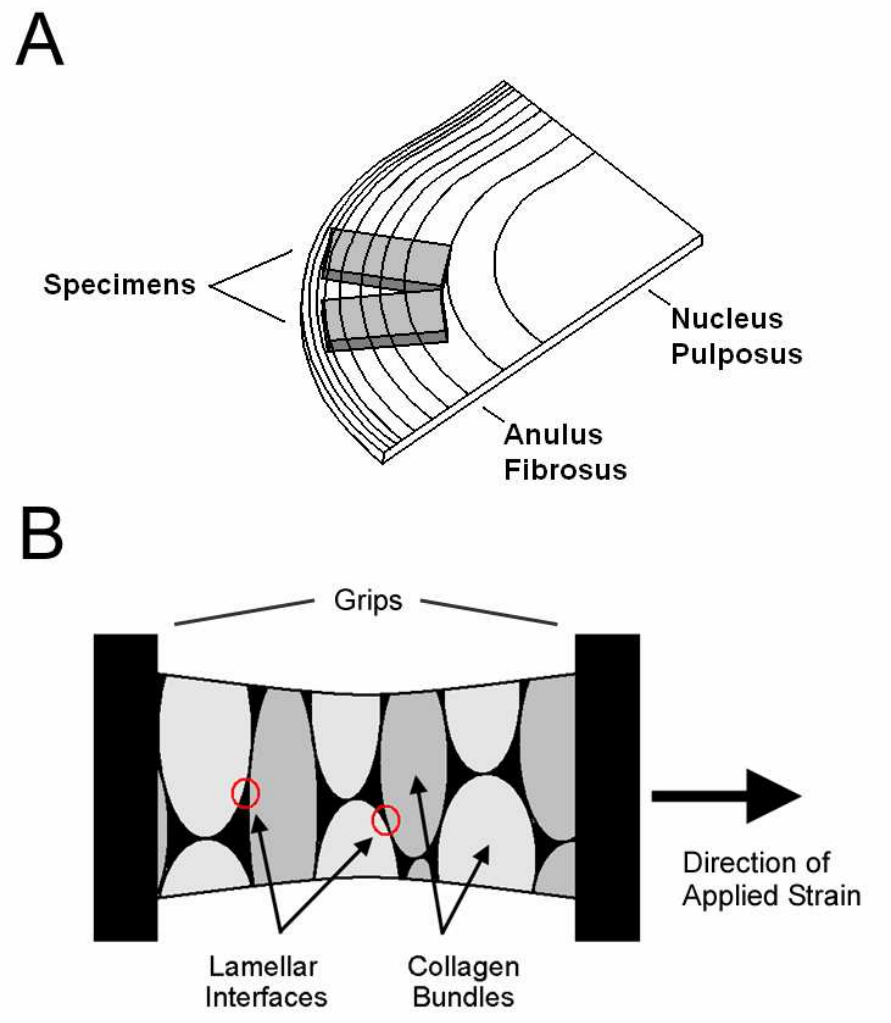


Figure 4.3. A. Intervertebral disc posterolateral quadrant schematic showing the harvest site for radially oriented specimens. B. Schematic of a strained specimen showing histological sampling sites within collagen bundles and at lamellar interfaces.

4.5.2 Results

Figure 4.4 illustrates splitting and subsplitting of collagen fibres within a lamella of a specimen subjected to radial tensile strain, in a manner consistent with that observed in a previous study (Pezowicz *et al.*, 2005). Elastic fibres within the lamellae of these specimens assumed a complex, multi-directional arrangement (Figure 4.5). Two distinct populations of fibres were indentified: those which were long, straight and aligned more towards the direction of the applied strain (labelled SE); and those which were shorter, relaxed or crumpled in appearance, and aligned more perpendicular to the direction of the applied strain (labelled RE). In several instances, an individual elastic fibre was observed to undergo a sharp change of direction along its length (Figure 4.6A, examples indicated by green circles). The pattern of elastic fibre arrangement observed in strained specimens was distinct when compared to that observed within the collagen bundles of adjacent unstrained specimens (Figure 4.6B), where the alignment of elastic fibres was largely unidirectional, and identical to that described in Chapter 3.

At lamellar interfaces in specimens under strain, where there was transverse lamellar separation, elastic fibres, both singularly and in bundles, were observed to maintain physical connections between those lamellae (Figure 4.7 and Figure 4.8). It was observed that these connections did not appear continuous along the length of the separated lamellae, but instead appeared to form points of adhesion at discrete locations (Figure 4.7). Where there was no lamellar separation, elastic fibres were observed as discrete ‘criss-cross’ meshworks, similar in appearance to those described in Chapter 3.

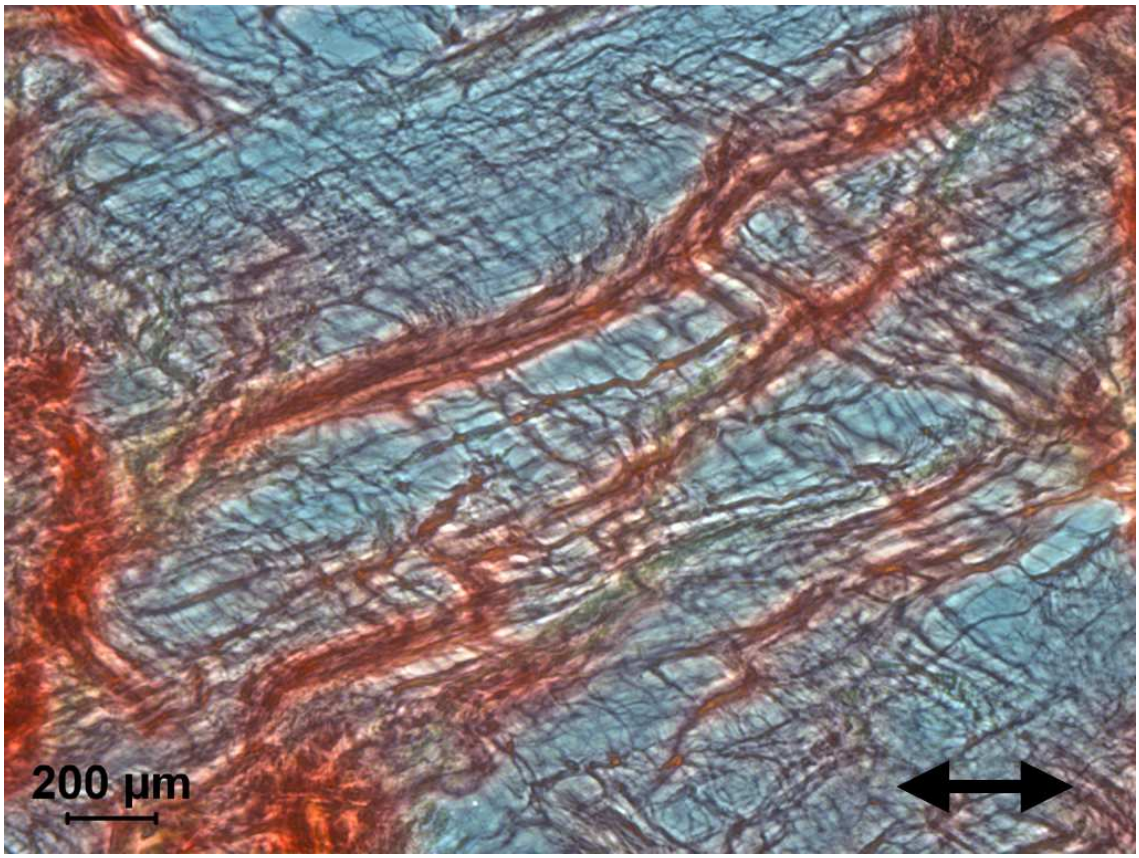


Figure 4.4 Transverse deformation of collagen bundles in specimens under radial tensile strain (arrows indicate test direction) resulted in splitting and sub-splitting of fibrous elements (stained red), in a manner comparable to that observed in a previous study (compare with Figure 1.4, (Pezowicz *et al.*, 2005)). (Van Gieson stain, phase contrast, 40 times objective magnification).

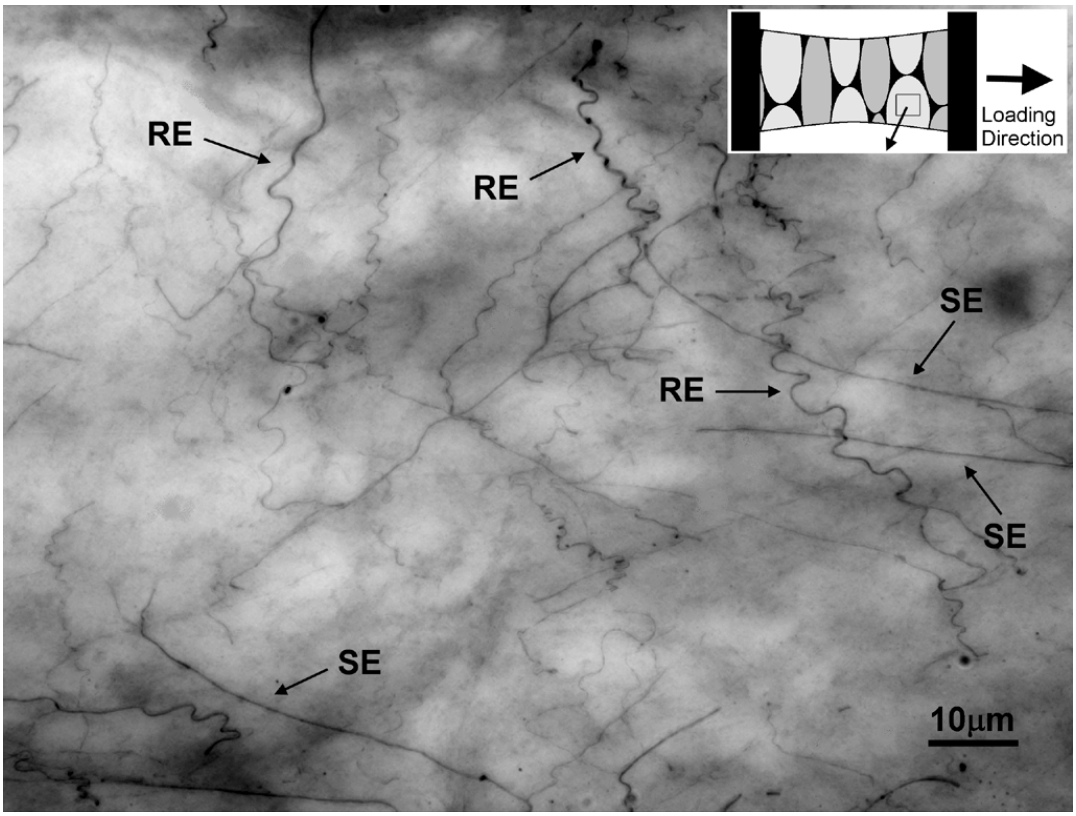


Figure 4.5. Elastic fibre network structure, within a collagen bundle, in the 40 year old, grade 2 specimen subjected to radial tensile strain (inset shows loading direction). *SE* = straight elastic fibres potentially indicating regions and directions where the collagen matrix is in tension. *RE* = relaxed elastic fibres potentially indicating regions and directions where the collagen matrix is in compression. (Resorcin-fuchsin stain, phase contrast composite z-stack image, 100x objective magnifcation).

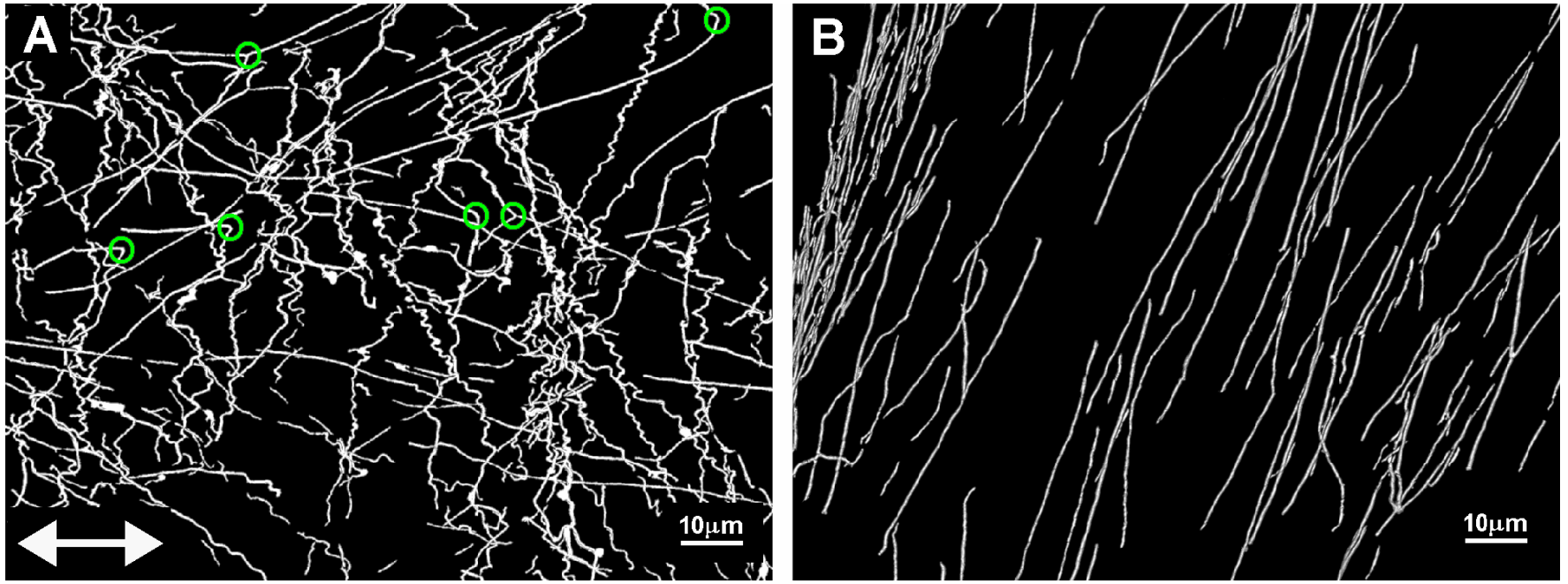


Figure 4.6. Comparison of elastic fibre arrangements within the collagen bundles of adjacent strained and unstrained specimens. A. Elastic fibre arrangement in a collagen bundle of a specimen subjected to radial tensile strain. Green circles indicate examples of elastic fibres that undergo sharp changes of direction along their length. Arrows indicate test direction. B. Elastic fibre arrangement in a collagen bundle of a specimen subjected to zero strain, displaying characteristic isotropy. Original images were z-series projections taken from 30 micron-thick sections stained with resorcin-fuchsin and imaged under phase contrast at 100 times objective magnification. Three-dimensional reconstructions of the elastic fibres in both images can be found on the accompanying media.

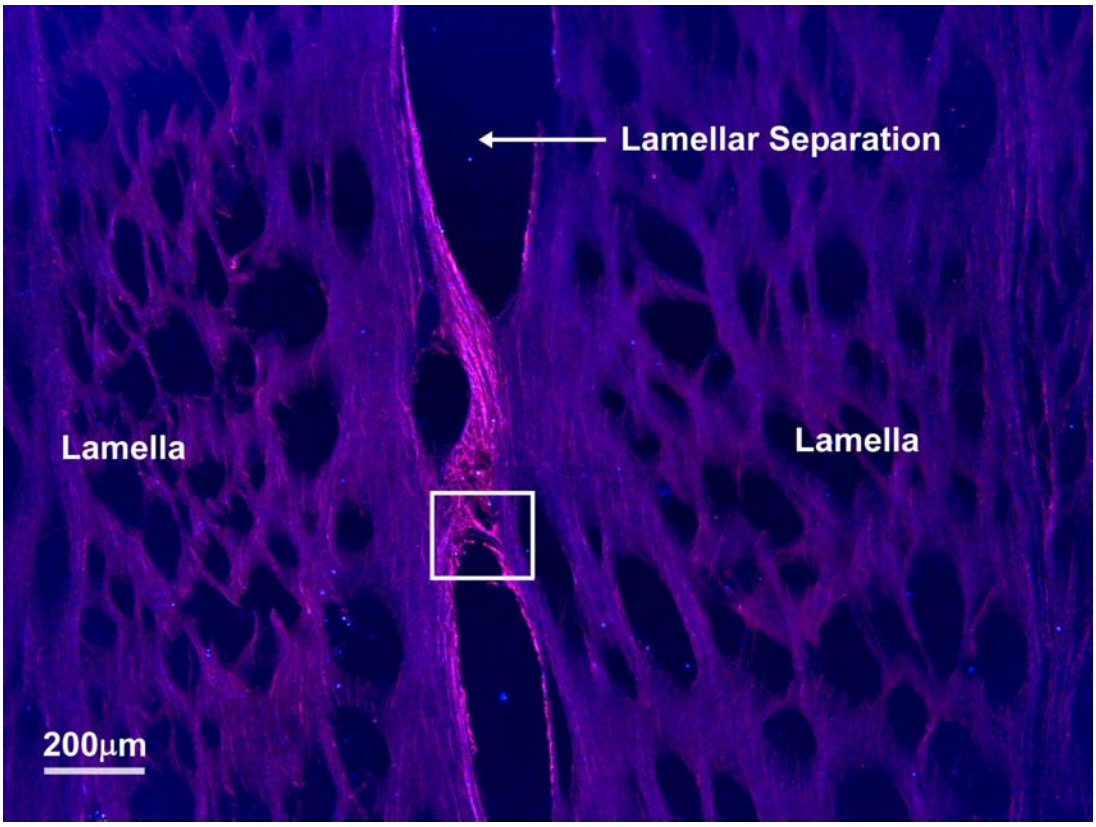


Figure 4.7. Elastic fibres (pink) form a point of adhesion between two lamella undergoing transverse separation in a specimen under radial tensile strain (40 year old, grade 2 specimen, dark field image, 30 micron section, resorcin-fuchsin stain). For the detail within the square refer to Figure 4.8.

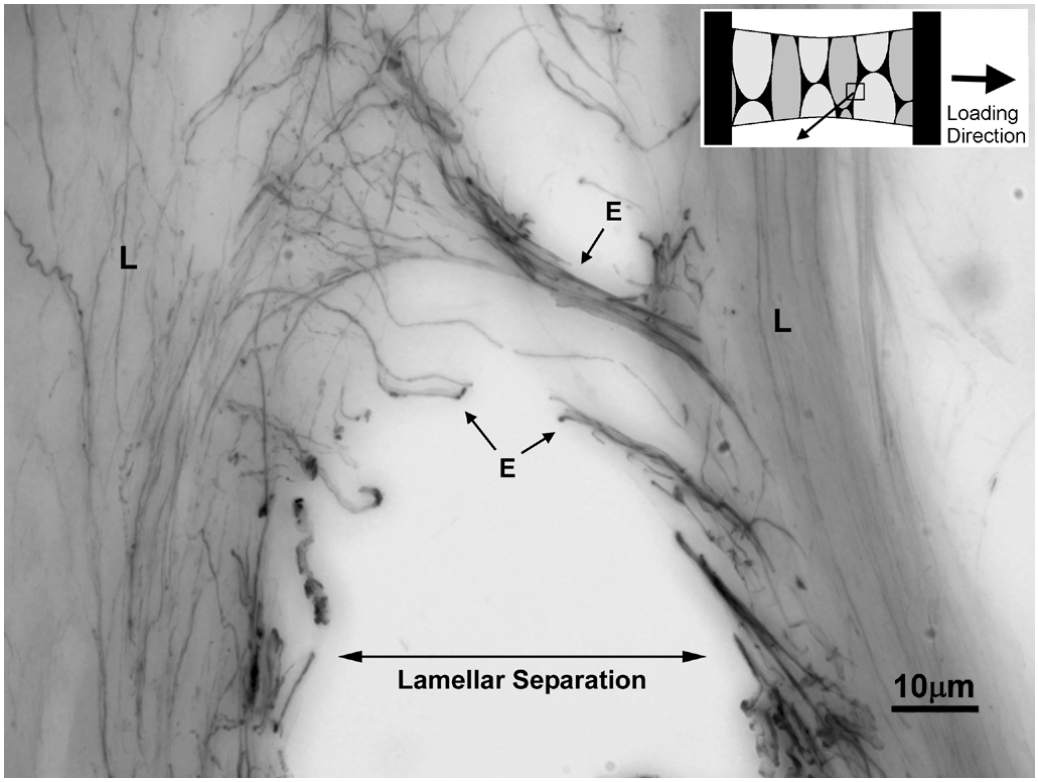


Figure 4.8. Bundles of elastic fibres, *E*, forming connections between two collagen bundles in consecutive lamellae, *L*, in a specimen subjected to radial tensile strain (inset shows loading direction). (40 year old, grade 2 specimen, resorcin-fuchsin stain, phase contrast composite z-stack image, 100x objective magnifcation). A three-dimensional reconstruction of the elastic fibres in this image can be found on the accompanying media.

4.6 Discussion

In this chapter, two experimental studies are described which examine the nature of the structure-function associations between elastic fibres and collagen in the context of the distinct mechanisms which facilitate tensile deformation of the anulus fibrosus extracellular matrix during physiological loading.

In the first study, the role of elastic fibres in maintaining collagen planar crimp was investigated using histochemistry and polarised light microscopy. This study was limited by the qualitative nature of the assessments – a quantitative study examining such parameters as crimp angle, amplitude and periodicity may have identified more nuanced differences. Indeed, qualitative comparisons of the images in Figure 4.2 appear to show variations in these parameters between and within specimens. Crimp morphology, however, has previously been shown to be heterogenous (Cassidy *et al.*, 1989). As a consequence, quantitatively demonstrating that variations in crimp morphology were due to the absence of elastic fibres rather than pre-existing heterogeneity would be problematic. Simply the observed presence or absence of crimp was therefore considered adequate to address the hypothesis proposed in this study.

The presence of collagen crimp consistently in all four specimens treated with elastase suggests that any role played by elastic fibres in its maintenance is minimal, supporting a rejection of the first null hypothesis proposed at the chapter outset. The inference to be made from these observations is that crimp is in fact an intrinsic structural property of anulus collagen fibres, and its existence is not dependent on the

presence of elastic fibres. This theory is consistent with the additional circumstantial evidence outlined in section 4.1.

In the second study, the potential for elastic fibres to provide connectivity, both between adjacent collagen fibres with lamellae, and between collagen fibre bundles in adjacent lamellae was investigated. A limitation of this study may have been the fact that during aqueous fixation, additional swelling of the tissue may have occurred, resulting in some distortion of the elastic fibres from their immediate post-strained configuration. In particular, bundle swell may have resulted in some decrease in lamellar separation. Also, the patterns of elastic fibre rearrangement may have been influenced by lack of in-situ boundary conditions for the collagen fibres.

Uniaxial strains applied to radially orientated anulus fibrosus specimens, perpendicular to the plane containing the collagen fibres, resulted in multidimensional rearrangement of intralamellar elastic fibres, supporting a rejection of the second null hypothesis proposed. Some fibres appeared long and straight, suggesting they were experiencing tension, and others shorter and crumpled, suggesting they were relaxed or experiencing compression (Figure 4.5). This pattern of arrangement stands in contrast to that observed in unstrained specimens, where alignment is largely uni-directional (Figure 4.6). Observations suggest that elastic fibres aligned parallel to collagen fibres maintain discrete points of connection between adjacent collagen fibres. It is possible that these points of connection are located at either the extreme ends of elastic fibres only, or at multiple locations along their lengths – the fact that a number of elastic fibres were observed to undergo sharp changes of transition along their length (Figure 4.6A) suggests that the second of these possibilities is the case. As collagen fibres reorient, it is plausible that when a decrease in the distance between

such point of connection occurs, the elastic fibre making those connections would crumple in the manner observed; such behaviour would also appear to suggest that these intralamellar elastic fibres are initially under a degree of pre-strain. Likewise, as the distance between connection points increases, elastic fibres would extend while maintaining a straight appearance. In both instances, as the relative positions of these connection points changes, so would the orientation of the elastic fibre, which is consistent with histological observations. These concepts are presented schematically in Figure 4.9, which illustrates simply how relative shear and normal strains between adjacent collagen fibres may result in both the crumpling and extension of the elastic fibres which inter-connect them. Additionally, the apparent predominant orientation of relaxed fibres transverse to the loading direction may be a consequence of the associated Poisson's ratio effects.

At the lamellar interface, elastic fibres were observed to maintain physical connections between collagen bundles in consecutive lamellae undergoing localised separation (Figure 4.8), supporting a rejection of the final null hypothesis proposed at the chapter outset. Evidence that fatigue related damage is commonly manifested as separation of anulus lamellae highlights the potential importance of these connections (Iatridis *et al.*, 2005). Importantly, elastic fibre connections were observed not to be continuous along the entire interface, but instead appeared to form discrete points of adhesion (Figure 4.7). The length of these adhesions should be considered with reference to the fact that in axial plane of the disc, collagen bundle cross-sections are oblique. It is therefore possible that these points of adhesion progress along the axis of the bundles into the plane of section. It is unclear from these results as to whether interlamellar connections are comprised of elastic fibres alone, or a combination of

elastic fibres and collagen – the inclusion of collagen would provide the connections with additional tensile strength. Elastin and collagen co-distribution at these locations could be investigated in a future study using immunohistochemistry.

The physiological relevance of cross-connecting elastic fibres within collagen fibre bundles is evident when considered in the context of the most common manifestations of matrix damage which have been observed following both fatigue loading and over-pressurisation (Iatridis and ap Gwynn, 2004; Iatridis *et al.*, 2005; Pezowicz *et al.*, 2006b). For example, in the absence of the elastic fibres which maintain adhesion between lamellae, the shear strains which occur as a result of relative reorientation between those lamellae in bending and torsion may increase the propensity for delaminations and circumferential tears to form. Within lamellae, in the absence of elastic fibres providing cross-collagen fibre connectivity, relative reorientation between adjacent collagen fibres could potentially occur more easily, and the restoration of the homeostatic configuration of those collagen fibres be less effective and less complete. A consequence of such a loss of cohesion may be progressive disorganisation within lamellae, which over time may enable radial fissures, including those that ultimately lead to nuclear prolapse, to propagate more easily.

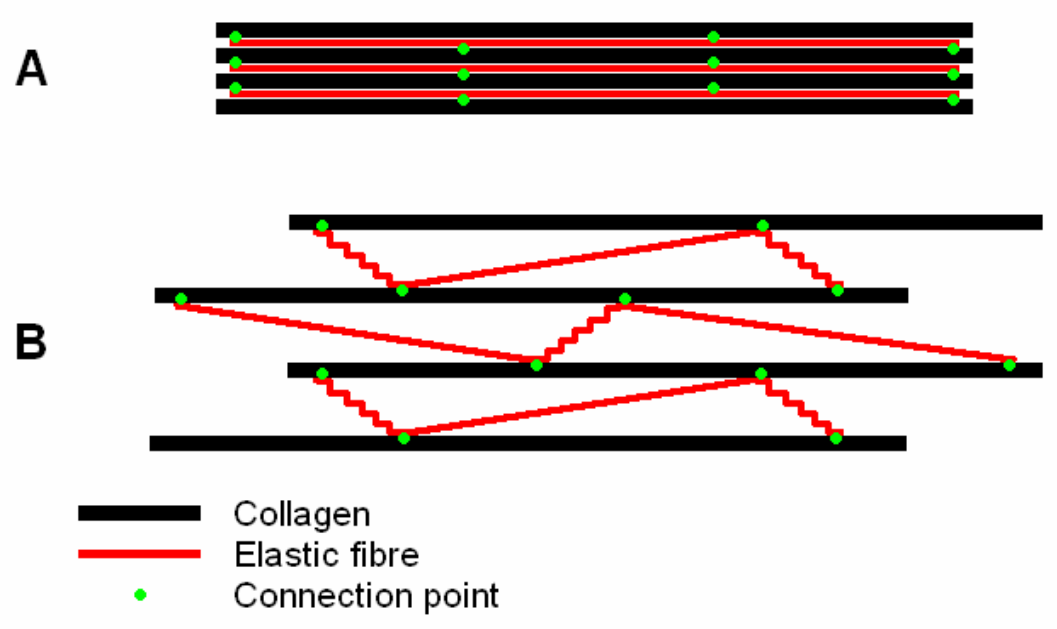


Figure 4.9. Schematic representating intralamellar elastic fibres and collagen fibres, with multiple points of connection between the them. A. In unloaded lamellae, elastic fibres lie parallel to collagen fibres. B. In loaded lamellae, relative shear and normal strains between adajcent collagen fibres results in decreased elastic fibre isotropy, and both localised fibre extension and crumpling.

CHAPTER 5: THE FUNCTIONAL ROLE OF ELASTIC FIBRES

5.1 Introduction

Detailed histological analyses of anulus fibrosus elastic fibre network structure have provided an important initial framework that has enabled researchers to theorise as to their possible functional roles. It has been suggested that elastic fibres may play a critical role in reinforcing the mechanical integrity of the collagen matrix and in facilitating its elastic recoil, both within and between collagen fibre bundles (Humzah and Soames, 1988; Yu, 2002; Yu *et al.*, 2002; Yu *et al.*, 2005; Yu *et al.*, 2007). The results of the studies described in previous chapters of this thesis significantly extend and refine this structural framework; however, direct experimental evidence of the exact nature and magnitude of the contribution made by elastic fibres to the mechanical behaviour of the anulus is required, and is the focus of this Chapter.

In Chapter 4, extension of anulus fibrosus specimens transverse to the predominant direction of the collagen fibres revealed that elastic fibres provide cross-connectivity between adjacent collagen fibres within lamellae, and between collagen fibres bundles in adjacent lamellae. These observations suggest that in the absence of elastic fibres, both intralamellar and interlamellar mechanical integrity would be weakened significantly. In this chapter, combinations of biochemically verified enzymatic treatments and biomechanical testing are employed to examine this possibility.

5.2 Scope

Following a statement of objectives and the hypotheses to be tested, this chapter is divided into three sections: specimen preparation and equilibration; development of targeted enzymatic treatments and validation of those treatments using biochemical assays; mechanical testing. Each of these sections begins with an introduction in which a detailed review of the literature is presented, including evaluation and selection of appropriate experimental techniques, followed by methods, results and discussion.

5.3 Objectives and Hypotheses

The objective in this chapter was to investigate the nature and magnitude of the contribution made by elastic fibres to the quasi-static mechanical properties of the anulus fibrosus in the radial direction, using a combination of biochemically validated targeted enzymatic treatments and biomechanical tests. Additional objectives were to examine how this role may vary with circumferential position and degenerative condition.

The following null hypotheses were proposed:

- Elastic fibres do not limit the extensibility of the anulus fibrosus in the radial direction.
- Elastic fibres do not enhance the initial elastic modulus of the anulus fibrosus in the radial direction.
- Elastic fibres do not enhance the ultimate elastic modulus of the anulus fibrosus in the radial direction.

5.4 Specimen Preparation and Equilibration

5.4.1 Review of Techniques

Preparation of small and precisely-dimensioned soft tissue specimens for mechanical testing poses a number of challenges. In this section, techniques used to overcome the most critical of these challenges are reviewed, evaluated and adapted for use in this study. Those challenges were specifically identified as: freezing and thawing effects; specimen preparation techniques; measurement of specimen initial dimensions; equilibration.

Freezing and Thawing Effects: Following collection of surgical or autopsy tissue specimens, it is almost always necessary to freeze them before further preparation. Additionally, it is commonly necessary to re-freeze them between final preparation and mechanical testing. Hickey and Hukins (1979) investigated the effects of deep freezing -35°C and freezing in liquid nitrogen to -195.8°C on the collagen fibril distribution in the anulus, and found no significant alterations in either case. The effect of long term freezing has not been investigated for isolated anulus fibrosus specimens, however it has been for complete functional spinal units. Three months of frozen storage at -18°C was found to result in no significant change to mechanical properties of ovine motion segments (Gleizes *et al.*, 1998). Canine motion segments frozen for 1 week at -80°C were found to suffer a loss of stiffness of between 1.8 percent and 12.1 percent, depending in the loading modality (Flynn *et al.*, 1990). In contrast, the elastic response of human motion segments was found not to be significantly affected after three weeks of storage at -20°C (Dhillon *et al.*, 2001). The compressive creep behaviour of porcine motion segments following frozen storage

was significantly altered (Bass *et al.*, 1997). It was suggested that the different results found for human and porcine discs could be attributed to differences in water content. The effects of frozen storage on the mechanical properties of soft tissues other than intervertebral disc have also been investigated. Long-term frozen storage has been found to have no effect on the biomechanical properties of ligaments (Woo *et al.*, 1986). In contrast, freezing tendons for 4 weeks at -30°C has been shown to signficantly alter their tensile failure properties and elastic modulus (Clavert *et al.*, 2001). Conflicting evidence therefore exists as to whether medium or long term frozen storage has any significant effects on tissue mechanical properties. From a practical perspective, frozen storage was essential in this investigation, as it is for most. To minimise inter-specimen variablity, all specimens were subjected to the same number of freeze-thaw cycles. The total number of cycles was limited to three: following autopsy retrieval, spines were stored at -70°C; spines were thawed for the removal of intervertebral discs, which were subsequently re-frozen at -30°C; finally, discs were thawed for grading and final specimen preparation, and specimens were then stored at -30°C until required for mechanical testing. Whilst frozen, specimens were kept wrapped in saline moistened gauze and double sealed in plastic bags or screw-top vials to prevent dehydration. All thawing was performed at room temperature.

Specimen Preparation Techniques: Prior to mechanical testing, it is critical that specimens be prepared with precise, uniform dimensions. Preparation is routinely performed in two stages: trimming the tissue to a uniform thickness; and cutting the specimen profile (e.g. rectangle or dumbell). The delicate nature of soft tissues poses a challenge with respect to the first of these steps, which has been overcome variously

by: embedding tissue in gelatin, freezing, then cutting uniform slices on a meat slicer (Wu and Yao, 1976); freezing tissue then trimming incrementally on a cryostat (freezing microtome) until uniform thickness is achieved (Acaroglu *et al.*, 1995; Ebara *et al.*, 1996; Elliott and Setton, 2001; Iatridis *et al.*, 2005); or cutting uniform slices using a vibratome (vibrating microtome) (Fujita *et al.*, 1997). For this study gelatin embedding was not considered a preferred option as the consequences for both mechanical properties and enzyme treatment efficacy were unknown. There is some question as to whether rapid freezing and thawing required for cryostat trimming may confound mechanical properties, although experimental evidence suggests such effects are insignificant (Galante, 1967); cryostat trimming was therefore selected for this study. The second step – cutting the specimen profile – is more straight forward, with methods typically involving a razor cutting tool of some kind, custom designed with the required profile (Acaroglu *et al.*, 1995; Ebara *et al.*, 1996; Fujita *et al.*, 1997; Elliott and Setton, 2001; Iatridis *et al.*, 2005). It was proposed that such a tool be constructed for this study. Additionally, cutting specimens while frozen limits peripheral compression-related damage.

Specimen Dimension Measurements: Accurate measurement of initial specimen width and thickness is required to calculate the cross-sectional area, to convert measured forces into stress. Techniques used in previous investigations for measuring dimensions include a laser sensor device (Elliott and Setton, 2001), an electrical conductivity sensor device (Skaggs *et al.*, 1994; Acaroglu *et al.*, 1995; Ebara *et al.*, 1996), a video extensometer (Holzapfel *et al.*, 2004) and a microscope combined with either a calibrated reticule, digital micrometer (Skaggs *et al.*, 1994; Acaroglu *et al.*, 1995; Ebara *et al.*, 1996) or calipers (Fujita *et al.*, 1997; Fujita *et al.*, 2000). Non-

contact dimension measurement techniques have obvious advantages over contact methods, in that specimen boundaries can be identified precisely and there is no potential for peripheral tissue deformation, such as that which may occur with calipers. Additionally, modern imaging technology provides the resolution necessary for high precision measurements. Non-contact dimension measurement using a digital imaging system was therefore considered most appropriate for this study.

Equilibration: Prior to testing, it is necessary to equilibrate specimens in saline until they reach a steady state level of hydration (Skaggs *et al.*, 1994; Acaroglu *et al.*, 1995; Ebara *et al.*, 1996; Fujita *et al.*, 1997; Elliott and Setton, 2001; Holzapfel *et al.*, 2004; Iatridis *et al.*, 2005; Wagner *et al.*, 2006). Circumferentially oriented specimens were found to reach greater than 95 percent of their equilibrium water content with 30 minutes (Acaroglu *et al.*, 1995; Ebara *et al.*, 1996). In contrast, single-lamellar specimens oriented parallel to the collagen bundles were found to reach 83 percent of equilibrium within 10 minutes, suggesting that equilibration time is related to specimen thickness (Skaggs *et al.*, 1994). As there were no published data with respect to the optimum equilibration times for radially oriented anulus fibrosus specimens, it was resolved to determine it experimentally (described in section 5.4.3).

5.4.2 Excision

Eight intervertebral discs from lumbar spines retrieved during autopsies, and excised and graded as described in section 2.2. All discs were from the L1-L2 level, and their grades, ages, and sexes are presented in Table 5.1.

Age	Sex	Grade
16	M	1
28	M	2
40	F	1
57	M	2
66	M	3
76	F	3
80	M	4
87	F	4

Table 5.1. Specimen age, sex and grade.

Each hemi-disc was divided into an anterolateral and posterolateral quadrant (Figure 5.1), the nucleus was separated from the anulus at the transition zone using a scalpel, and the endplate was carefully removed. Each anulus quadrant was then mounted on a cryostat chuck using OCT compound (Figure 5.2), and snap frozen in liquid nitrogen. The chuck was placed in the cryostat (Miles Laboratories, Elkhart, Indiana USA), and 5 μm slices were taken incrementally, until the cutting surface was approximately 1mm from the mid-plane of the disc (assessed qualitatively). The specimen was then removed from the chuck by allowing the OCT mounting compound to thaw, flipped and re-adhered by submerging in liquid nitrogen. 5 μm slices were taken

incrementally from this opposite side until a uniform thickness of between 1 and 2 mm was achieved, measured using digital callipers, then removed from the chuck.

To enable specimens of uniform dimensions to be cut consistently, a custom razor-blade cutting tool was designed and constructed from aluminium. The tool was able to cut either parallel-edged (as used in this study) or dumbbell shaped specimens, simply by reversing the two blade mounting components. Figure 5.3A illustrates the cutter configured to cut dumbbell shaped specimens, and Figure 5.3B illustrates the cutter configured to cut parallel edged specimens.

Using this tool, two adjacent parallel-edged strips approximately 5 mm wide were cut from the centre of each quadrant (whilst still frozen to prevent excessive lateral deformation). Specimens were then trimmed using a scalpel to an approximate length of 10 mm, and washed thoroughly in saline to remove all OCT mounting compound. Finally, specimens were individually wrapped in saline moistened gauze, sealed in 5 ml plastic screw-top specimen tubes and frozen at -30°C until required for mechanical testing.

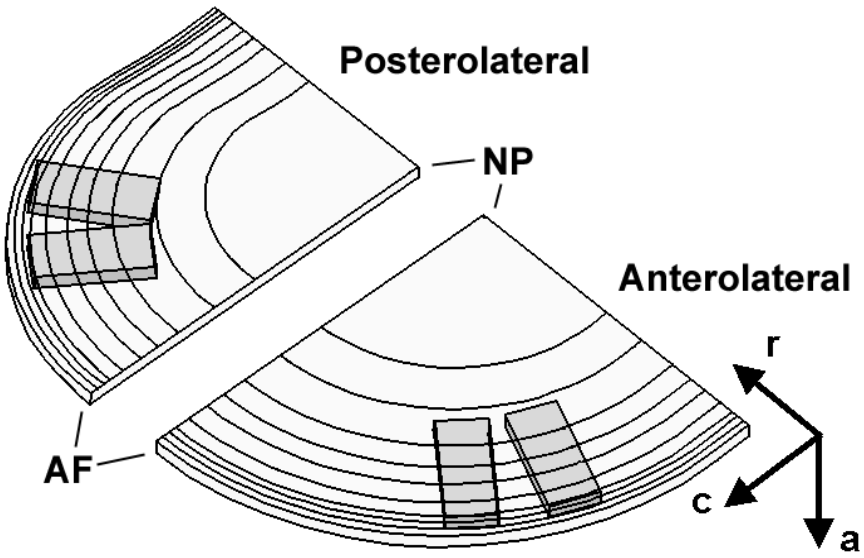


Figure 5.1. Hemi-disc schematic illustrating specimen harvest sites in the anterolateral and posterolateral quadrants (r = radial, c = circumferential and a = axial directions).



Figure 5.2 Anulus quadrant mounted on cryostat chuck ready for trimming.

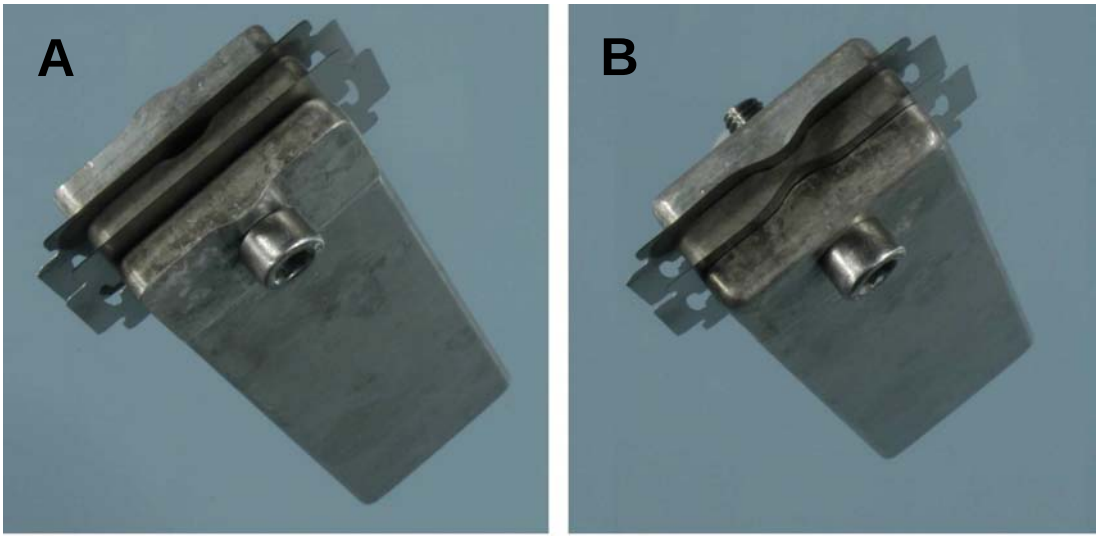


Figure 5.3 Razor tool, configured to cut A. parallel-edged specimens or B. dumb-bell shaped specimens.

5.4.3 Equilibration

Six specimens, separate from the primary cohort but identical in their method of preparation were weighed immediately following excision. They were each then submerged in 2 ml of 0.15 M PBS at 4°C, and re-weighed after 30 minutes, after 60 minutes and after 90 minutes. Prior to each weighing, excess fluid was carefully removed from the surface of specimens by quickly dabbing with blotting paper. A one-way repeated measures analysis of variance was performed to test for significant changes in specimen wet weight (hydration) at each time interval. Post-hoc analyses with Bonferroni corrections were used to determine the time intervals between which significant changes occurred.

The analysis of variance indicated significant differences in specimen wet weights were present at different time intervals ($p < 0.0001$). A summary of results with post-hoc analyses is provided in Table 5.2.

Specimen wet weight increased by a significant 9.8 percent over the first 30 minutes of equilibration. Between 30 and 60 minutes, wet weight increased by a further, but statistically insignificant 3.7 percent, and between 60 and 90 minutes by a further, but still statistically insignificant 0.9 percent. Figure 5.4 charts the time course of specimen hydration, as percent increase in wet weight (from the zero time point). Data points represent mean ± standard deviation.

Time Interval (Minutes)	Wet Weight (g, mean±SD)	Change in Wet Weight		Significance Change (P < 0.05)
		(g, mean±SD)	Percent	
0	0.084±0.007	-	-	-
30	0.092±0.012	+0.008±0.005	+9.8	Yes
60	0.096±0.013	+0.003±0.002	+3.7	No
90	0.097±0.015	+0.001±0.002	+0.9	No

Table 5.2. Results of specimen hydration study (n = 6).

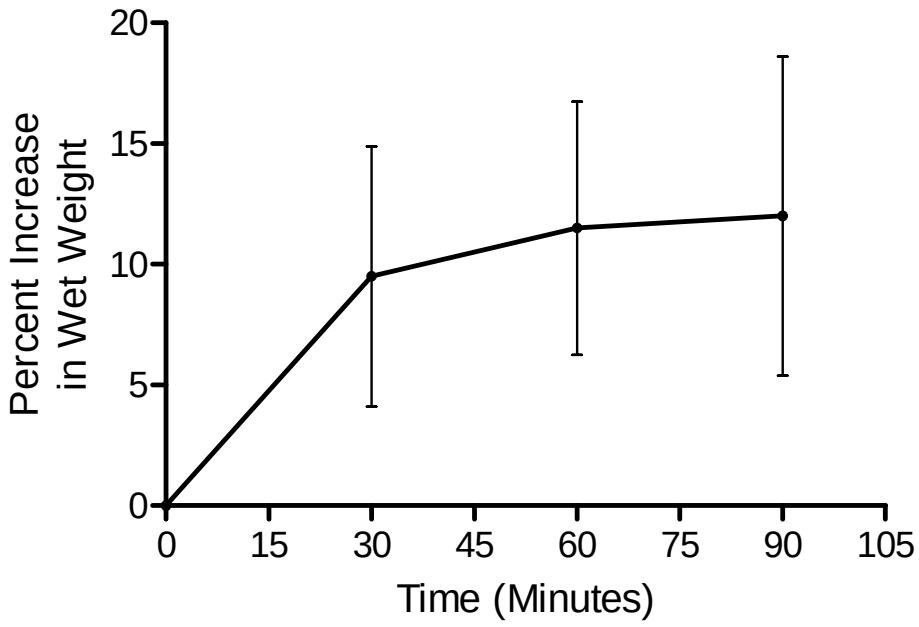


Figure 5.4. Time course percent increase in specimen wet weight (measured from the zero time point). Mean ± SD, n = 6.

The results of this hydration study demonstrate that after 30 minutes there is no further statistically significant change in specimen wet weight. After this time interval, specimen hydration was approximately 95 percent of hydration relative to the 90 minute time point. While the increase of 3.7 percent between 30 minutes and 60 minutes was not statistically significant, the variability in the magnitudes of change were quite large for the small specimen cohort (n = 6). It was therefore decided to extend equilibration time to 60 minutes, which equated to approximately 99 percent of hydration relative to the 90 minute time point.

In summary, based on these results, each specimen was equilibrated in 2 ml of 0.15 M phosphate buffered saline at 4°C for 60 minutes, prior to the measurement of dimensions, and again prior to each mechanical test.

It was recognised that following enzyme treatments, changes to tissue structure and chemistry may have resulted in changes to equilibration times. However, as specimens were predicted to lose a proportion of their glycosaminoglycans (responsible for maintaining tissue hydration), time to equilibrium hydration was considered likely to decrease, not increase, and as such, 60 minutes was still considered appropriate.

5.4.4 Dimension Measurements

Following saline equilibration, dimensions (width and thickness) were measured using a custom built, high resolution vision system. The system consisted of a monochrome digital fire-wire camera (Sony Electronics Inc., Tokyo, Japan), with lens and extension tube (Navitar Inc., Rochester, NY, USA) giving a measurement resolution of ± 10 μm. Specimens were illuminated from above using incandescent lamps and from below using a light box to provide maximum contrast. The system was calibrated using a microsope calibration slide with 10 μm divisions, with the number of pixels per micron determined using image analysis software (ImageJ; National Insitutes of Health, USA).

Thickness and width (Figure 5.5) were measured on each side of the specimen at eight separate locations along its length and averaged. Dimensions were measured both prior to enzyme treatment and following enzyme treatment, and the significance of any changes to cross-sectional area assessed.

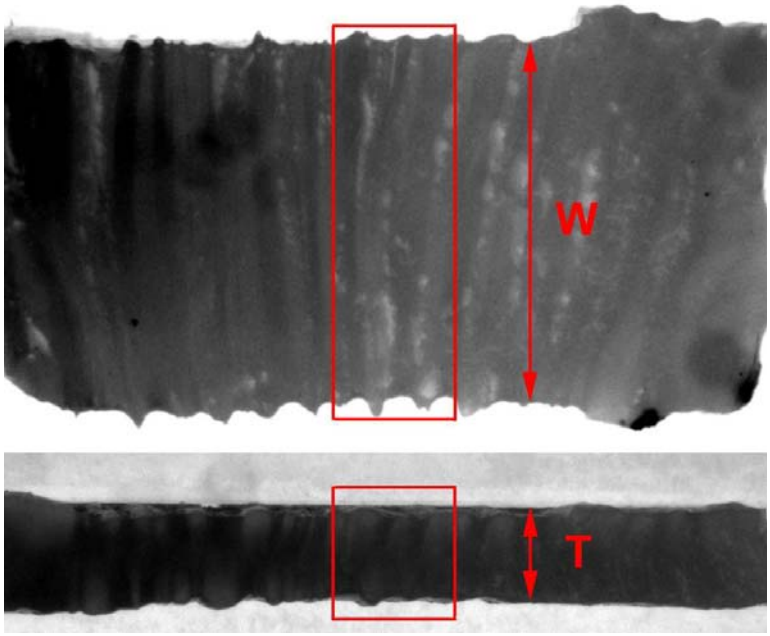


Figure 5.5. Example specimen images used for dimension measurements. W = width, T = thickness. The rectangle indicates the approximate location of the gauge region.

5.5 Development and Validation of Enzyme Treatments

5.5.1 Introduction

Targeted enzymatic degradation is a technique in which enzyme treatments are used to remove specific elements of the extracellular matrix while leaving other elements intact. Conducted in combination with biomechanical tests, targeted enzymatic degradation is a valuable tool for investigating the functional roles of the individual constituents of composite biological tissues.

These techniques have been used successfully on a variety of such tissues to stratify their mechanical behaviours in terms of the unique contributions of collagen (Oxlund and Andreassen, 1980; Yuan *et al.*, 2000; Rieppo *et al.*, 2003; Wayne *et al.*, 2003), glycosaminoglycans (Oxlund and Andreassen, 1980; Bader *et al.*, 1981; Viidik *et al.*, 1982; Schmidt *et al.*, 1990; Torzilli *et al.*, 1997; Chan *et al.*, 2001; Rieppo *et al.*, 2003; Wayne *et al.*, 2003; Basalo *et al.*, 2005; Perie *et al.*, 2006a; Perie *et al.*, 2006b; Yerramalli *et al.*, 2007) and elastin (Karlinsky *et al.*, 1976; Missirlis, 1977; Oakes and Bialkower, 1977; Oxlund and Andreassen, 1980; Viidik *et al.*, 1982; Oxlund *et al.*, 1988; Yuan *et al.*, 2000; Lee *et al.*, 2001; Rieppo *et al.*, 2003; Black *et al.*, 2005). These tissues have included skin (Oxlund and Andreassen, 1980; Oxlund *et al.*, 1988), tendon (Missirlis, 1977; Oakes and Bialkower, 1977; Viidik *et al.*, 1982), articular cartilage (Bader *et al.*, 1981; Schmidt *et al.*, 1990; Torzilli *et al.*, 1997; Rieppo *et al.*, 2003; Wayne *et al.*, 2003; Basalo *et al.*, 2005), lung (Karlinsky *et al.*, 1976; Yuan *et al.*, 2000), aortic valve (Missirlis, 1977; Lee *et al.*, 2001), vocal fold (Chan *et al.*, 2001), artery (Armeniades *et al.*, 1973; Oxlund and Andreassen, 1980; Viidik *et al.*, 1982) and intervertebral disc (Perie *et al.*, 2006a; Perie *et al.*, 2006b; Yerramalli *et al.*,

2007). Enzyme treatment conditions vary considerably between studies, in some cases apparently arbitrarily and in other cases more specifically to reflect the unique distributions and quantities of the matrix elements under analysis. The efficacy of enzyme treatments has most frequently been established biochemically (Missirlis, 1977; Oxlund and Andreassen, 1980; Oxlund *et al.*, 1988; Schmidt *et al.*, 1990; Torzilli *et al.*, 1997; Lee *et al.*, 2001; Rieppo *et al.*, 2003; Wayne *et al.*, 2003; Basalo *et al.*, 2005; Black *et al.*, 2005; Perie *et al.*, 2006b; Yerramalli *et al.*, 2007) or, less often, histologically (Karlinsky *et al.*, 1976; Oakes and Bialkower, 1977; Torzilli *et al.*, 1997; Chan *et al.*, 2001; Rieppo *et al.*, 2003) with varying degrees of rigour, and in some cases not at all (Yuan *et al.*, 2000). A subset of those studies that included such analyses presented results quantitatively as evidence of the efficacy of their enzymatic treatments (Missirlis, 1977; Oxlund and Andreassen, 1980; Bader *et al.*, 1981; Torzilli *et al.*, 1997; Lee *et al.*, 2001; Rieppo *et al.*, 2003; Wayne *et al.*, 2003; Basalo *et al.*, 2005).

5.5.2 Review of Techniques

5.5.2.1 Treatments

The principle challenge associated with enzyme degradation techniques is to ensure that treatments effect only those matrix elements being targeted, or, alternatively where there is demonstrated non-specific degradation, that these effects are accounted for by some means. In this section the techniques that have been used to address these and other challenges are reviewed and evaluated.

Oxlund et al. (1985) studied the role of elastin in the mechanical properties of rat skin. The elastin content of skin is less than one percent in terms of dry weight. The treatment developed in this study used porcine pancreatic elastase combined with soybean trypsin inhibitor to reduce the collagenolytic activity of the enzyme. The effect of the treatment of tissue elastin was assessed both gravimetrically and by amino acid analyses of crosslinking desmosine and isodesmosine, comparing quantities in digested specimens compared with controls. Collagen degradation was assessed both by gel-electrophoresis, and by evaluating changes in the mechanical properties of tissue-engineered collagen films before and after digestion. Treatments were found to reduce elastin content by approximately 59 percent while leaving collagen unaffected.

Lee et al. (2001) studied the role of elastin in the mechanics of the porcine aortic valve, in which it constitutes approximately 13 percent of the dry weight. The treatment in this study used elastase (type unspecified) combined with soybean trypsin inhibitor. Successful elastin degradation was assessed using a fluorescence assay for desmosine and isodesmosine, and collagen degradation was assessed by measuring

hydroxyproline loss. The protocol was found to completely solubilise elastin, while leaving collagen unaffected.

Oakes and Bialkower (1977) studied the role of elastin in the mechanical properties of the elastic wing tendons of domestic fowls. Specimens were treated using purified elastase with penicillin sodium and streptomycin sulphate as bacterial inhibitors. Soybean trypsin inhibitor to prevent collagenolytic activity was not included, however a previous study (Bialkower, 1974) was referenced in which the collagenolytic activity of the elastase used was shown to be minimal. Successful digestion of elastin was verified by examining the tissue ultrastructure before and after treatment.

Missirlis (1977) examined the role of elastin in the mechanical properties of human, canine and bovine aorta, human aortic valve and canine hind limb tendon. Preliminary studies were performed to determine the optimal conditions for removal of elastin without causing damage to collagen, with results indicating that 0.3 mg of pancreatic elastase and 0.3mg of soybean trypsin inhibitor, pH 8.8 at room temperature, removed 98 percent of elastin and only four percent of collagen (measured as hydroxyproline).

Yuan et al. (2000) described the effects of pancreatic elastase and collagenase treatments on the mechanical properties of lung tissue strips. The mechanical properties were tested before and after 60 minutes and 30 minutes of elastase and collagenase treatment respectively. No biochemical or histological verification of the efficacy of these enzyme treatments was described, nor were possible effects of glycosaminoglycan loss assessed.

Of these five studies only three attempted to minimise non-specific degradation of collagen by including soybean trypsin inhibitor in the incubation solution. The treatment conditions for these studies are summarised in Table 5.3. The differences in enzyme concentration between the studies of Oxlund et al. (1998) and Lee et al. (2001) may be explained by the relative total amounts of elastin in each of the tissues under analysis, in addition to distinct patterns of matrix codistribution and structural integration. Reasons for the difference in soybean trypsin inhibitor concentration relative to enzyme concentration are less obvious, but may plausibly be due to differences in the tested, stated or perceived tryptic activity of the enzyme being used. The reported elastin content of the human anulus fibrosus is approximately two percent, although it increases with degeneration (Cloyd and Elliott, 2007). An enzyme concentration slightly greater than that used for skin, which contains one percent elastin, was therefore considered appropriate, with other conditions (temperature, soybean trypsin inhibitor concentration, pH and incubation time) identical.

While the degradative effects of elastase on collagen can be minimised using soybean trypsin inhibitor, the effects on glycosaminoglycans cannot. It is therefore critical to be able to separate the effects of elastin loss from those resulting from any accompanying glycosaminoglycan loss. Of the studies referred to in Table 5.3, only one accounted for mechanical changes resulting from the non-specific degradation of glycosaminoglycans by their elastase treatment (Lee *et al.*, 2001). To achieve this, a separate cohort of specimens was digested with the enzyme trypsin, and the resulting changes to mechanical properties compared to those in specimens treated with elastase. The authors were then able to describe clear differences in the changes in mechanical properties between the two groups. Their stated reason for selecting

trypsin for glycosaminoglycan digestion was that it has no effect on tissue collagen or elastin. There is, however, evidence that trypsin can degrade elastic fibre associated microfibrillar proteins such as fibrillin (Kielty *et al.*, 1994). As microfibrils act as a structural scaffold for the elastin protein in mature elastic fibres, it is possible that their disruption would leave elastic fibres mechanically compromised, more so with respect to elaunin and oxytalan elastic fibres, of which microfibrils form a greater relative proportion (Kielty *et al.*, 2002).

An alternative enzyme to trypsin is chondroitinase ABC, which effectively and specifically degrades chondroitin sulphate glycosaminoglycans, hyaluronan and dermatan sulphate (Yamagata *et al.*, 1968). A limitation of this enzyme is that it does not specifically degrade keratan sulphate, which consitutes a significant proportion of the total glycosaminoglycan content of the anulus (Adams and Muir, 1976). It has however been used extensively to investigate the specific roles of glycosaminoglycans in the tensile and compressive mechanical properties of connective tissues.

Chondroitinase ABC has been used previously to investigate the roles of glycosaminoglcyans in intervertebral discs, both at the tissue level (Perie *et al.*, 2006b) and in motion segments (Yerramalli *et al.*, 2007). Chondroitinase ABC treatments have also been used to examine the role of glycosaminoglycans in the tensile mechanical properties of human femoral condylar cartilage (Kempson *et al.*, 1973) and articular cartilage, (Schmidt *et al.*, 1990; Basalo *et al.*, 2005) and on solute mobility in articular cartilage (Torzilli *et al.*, 1997). In each of these studies, the depletion of the majority of glycosaminoglycans was verifed using biochemical assays.

Table 5.4 summarises chondroitinase ABC treatment conditions used in each of these studies. The wide variability in parameters, particularly enzyme concentration, emphasises the need for quantitative biochemical verification of satisfactory glycosaminoglycan depletion prior to application. It was considered important that environmental conditions (temperature and incubation time) match those used for elastase treatments as closely as possible, so that any consequences of these parameters for tissue mechanical properties would be similar irrespective of treatment group. An enzyme concentration of 1 unit per ml (the highest of those listed in Table 5.4) was adopted to ensure adequate glycosaminoglycan depletion.

Study	Elastase Concentration	SBTI* Concentration	Incubation Time	Incubation Temperature	pH
Missirlis *et al*. (1977) (Run #24)	0.33 mg/ml	0.33 mg/ml	5 hours	22°C	8.8
Oxlund *et al*. (1988)	1 unit/ml	3 mg/ml	36 hours	37°C	8.6
Lee *et al*. (2001)	60 units/ml	0.1mg/ml	36 hours	37°C	8.6

Table 5.3. Elastin degradation conditions used in previous studies. *Soybean trypsin inhibitor.

Study	Chondroitinase ABC Concentration	Incubation Time	Incubation Temperature	pH
Perie *et al*. (2006b)	0.125 units/ml	24 hours	25°C	8.0
Kempson *et al*. (1976)	1 unit/ml	48 hours	37°C	8.0
Torzilli *et al*. (1997)	1 unit/ml	48 hours	37°C	8.0
Basalo *et al*. (2005)	0.1 units/ml	24 hours	37°C	8.0
Schmidt *et al*. (1990)	0.125 units/ml	24 hours	25°C	8.0
Yerramalli *et al*. (2007)	0.25 units/ml	12 hours	37°C	*

Table 5.4. Glycosaminoglycan degradation conditions used in previous studies. *pH not stated.

5.5.2.2 Validation

To validate the efficacy of the elastase treatment it was necessary to confirm biochemically that the majority of the elastic fibres had been degraded. Additionally, it was essential to ensure that the elastase treatment had minimal degradative effects on the tissue collagen. Finally, it was necessary to quantify the non-specific loss of glycosaminoglycans by the elastase treatment and to ensure that the complimentary chondroitinase ABC treatment resulted in a comparable loss.

The most readily measurable component of elastic fibres is elastin, or more specifically, a unique marker of solubilised elastin. As described in section 1.2.2.1, desmosine and isodesmosine are crosslinking amino acids unique to elastin. Variations on three techniques for measuring desmosine predominate in the literature – high performance liquid chromatography (HPLC) (Covault *et al.*, 1982), radioimmunoassay (RIA) (Starcher, 2001) and enzyme linked immunosorbent assay (ELISA) (Verplanke *et al.*, 1988; Watanabe *et al.*, 1989; Osakabe *et al.*, 1995). A comparison of two of these techniques, HPLC and competitive ELISA, demonstrated that the ELISA was capable of measuring as little as 6 pmol/ml of desmosine, compared with 95 pmol/ml for HPLC, and thus had the advantage of greater sensitivity (Osakabe *et al.*, 1995). For this reason a competitive ELISA was selected as the preferred measurement technique.

Hydroxyproline is an established marker of solubilised triple-helical collagen. A widely used, simple and robust colourimetric technique was used to measure hydroxyproline in this study (Stegemann, 1958). Hydroxylysylpyridinium crosslinks (pyridinoline) are mature enzymatic crosslinks unique to collagen (Eyre *et al.*, 1988).

Measurement of pyridinoline was therefore considered appropriate to assess crosslink degradation as a result of the elastase treatment. A published high performance liquid chromotographic method was used as a basis for the development of the technique used in this study (Eyre *et al.*, 1988).

Uronic acid is a unique marker of solubilised glycosaminoglycans, keratan sulphate being an exception (Nelson and Cox, 2005). Due to the lack of a sufficiently robust alternative which included an assessment of keratan sulphate degradation, measurement of uronic acid using an established colourimetric technique was considered the most appropriate for this study (Blumenkrantz and Asboe-Hansen, 1973).

5.5.3 Methods

5.5.3.1 Treatments

Elastin was selectively degraded from the tissue matrix using an optimised version of the established techniques described in section 5.5.2.1. One specimen from each quadrant was incubated in a solution consisting of 3 U of high purity pancreatic elastase in 1 ml of 0.2 M Tris-HCl, pH 8.6, with 10 mM N-ethylmaleimide and 5 mM benzamidine hydrochloride as protease inhibitors. Additionally, 3 mg of soybean trypsin inhibitor was included to limit non-specific degradation of collagen by the elastase.

To account for the predicted effects of non-specific degradation of glycosaminoglycans by elastase, the second, adjacent specimen from each quadrant was incubated in a solution consisting of 1 U of chondroitinase ABC in 1 ml of 0.05 M Tris-HCl plus 0.06 M sodium acetate buffer, pH 8.0, with 10 mM N-ethylmaleimide and 5 mM benzamidine hydrochloride and 1 mM phenylmethanesulfonyl fluoride as protease inhibitors, to specifically degrade glycosaminoglycans while leaving elastic fibres and collagen unaffected. Both treatments were carried out for 36 hours at 37°C under gentle agitation.

Following treatment, specimens were washed for 30 minutes in 0.15 M phosphate buffered saline; washes were then combined with extracts for biochemical validation analyses as required. All reagents were obtained from Sigma-Aldrich, St Louis, MO, USA.

5.5.3.2 Validation

Validation of the described treatments was performed in a preliminary experiment, using four specimens (per treatment group) separate from the primary cohort but identical in their method of preparation. Sources of all reagents are listed in Appendix 5.

Following treatment, but prior to assays being conducted, tissue fragments were completely digested for 24 hours at 56°C in 2 ml of a solution containing 100 μg of proteinase K buffered with 100 mM di-potassium hydrogen orthophosphate at pH 8.0. 1 ml each of proteinase K digested tissues, and of combined extracts plus wash solutions were then subjected to 24 hours of hydrolysis in 6 M hydrochloric acid at 110°C. Aliquots of hydrolysed solutions were used for desmosine, hydroxyproline and pyridinoline assays. Aliquots of unhydrolysed solutions were used for uronic acid assays.

5.5.3.2.1 Desmosine Assay

The protocol described here was adapted from a previous study (Osakabe *et al.*, 1995). A number of minor modifications were made based on the availability of reagents. Specifically, bovine serum albumin (BSA) was substituted for casein and the substrate, tetramethylbenzidine (TMB) was replaced with *o*-phenylenediamine (OPD) due to its extremely high sensitivity (~7 pg/well). Consequentially, absorbance was read at 490 nm instead of 450 nm. These modifications were not expected to significantly alter the efficacy of the assay, however, it was found that the prescribed concentration of the initial antigen of 1 μg/ml produced insufficient color generation with OPD. As a consequence, an initial experiment was performed in which serial

dilutions of this antigen, albumin conjugated desmosine, were assayed directly. Results indicated a higher concentration of 16 μg/ml was necessary for adequate colour generation.

The assay itself was then carried out according to the following procedure: the wells of a round-bottom polystyrene microtitre plate were each coated with 50 μl of albumin conjugated desmosine at a concentration of 16 μg/ml, and the plate was sealed and incubated for 24 hours at 4°C. The wells were then washed three times with phosphate buffered saline (PBS), pH 7.4, containing 0.05 percent TWEEN 20, 100 μl/well of 1 percent BSA in PBS was added and the plate was incubated for one hour at room temperature to block remaining unbound sites. 1 in 400 diluted antidesmosine-KLH in 1 percent BSA in PBS was mixed in equal volume with 1 in 10 diluted samples, and desmosine standards, and incubated for 1 hour at room temperature. The wells of the plate were again washed, and 50 μl/well of the sample (or standard) plus antibody mixture was added. The plate was then sealed and incubated for 24 hours at 4°C. The wells were washed, 50 μl/well of 1 in 1000 diluted HRP labelled antirabbit immunoglobulins in 0.5 percent BSA in PBS was added and the plate was incubated for 90 minutes at room temperature. The wells were washed a final time, and 100 μl/well of OPD substrate solution was added. Once sufficient colour had developed (after approximately eight minutes), the reaction was terminated with 100 μl of 0.5 M sulphuric acid, and absorbance was read at a wavelength of 490 nm on a microplate reader (Wallac 1420, Perkin Elmer Inc, Waltham, MA, USA). All samples and standards were assayed in triplicate and the mean absorbance was calculated.

5.5.3.2.2 Hydroxyproline Assay

Hydroxyproline was measured using established methods (Stegemann, 1958). 100 µl aliquots of sample or standard were combined with 1.9 ml of deionised water in glass test tubes. 4 ml of freshly made chloramine-T solution (1.4 g chloramine-T in 190 ml deionised water, 50 ml propan-2-ol, and 40 ml of citrate buffer solution containing 33.6 g anhydrous sodium acetate, 57.5 g tri-sodium citrate hydrate and 5.5 g citric acid in 385 ml propan-2-ol and 615 ml deionised water, adjusted to pH 6.25) were then added to each tube and vortexed. After six minutes, 2 ml of freshly made p-dimethylaminobenzaldehyde solution (15.75 g p-dimethylaminobenzaldehyde in 7.5 ml deionised water, 41.25 ml concentrated hydrochloric acid and 135 ml propan-2-ol) were added to each tube, which were then capped and inverted vigorously to mix. Tubes were then incubated in a water bath at 60°C for 20 minutes, cooled in tap water for 30 minutes, and allowed to stand in air for 15 minutes. Finally, absorbance was read on a spectrophotometer (Ultraspec 2100 Pro, Amersham, Little Chalfont, UK) at a wavelength of 560 nm. Four serial dilutions of hydroxy-d-proline and a blank (deionised water) were used to generate standard curves.

5.5.3.2.3 Pyridinoline Assay

Pyridinoline was measured using reversed-phase high performance liquid chromatography (HPLC). Standards, being a mixture of pyridinoline and deoxypyridinoline, were a gift from the Division of Clinial Biochemistry at the Insititute of Medical and Veterinary Science. The methodology was adapted from a previous study (Eyre *et al.*, 1984) and existing internal procedures. The HPLC system consisted of a 250 x 4.6 mm C18 column fed via a matching guard column (SGE Analytical Science Pty Ltd, Ringwood, Australia) by a binary pump through a

degassing module and outputting to a fluorescence detector (Agilent Technologies Inc, Santa Clara, CA, United States) with excitation and emission wavelengths of 285 nm and 397 nm respectively. Initially, a mobile phase with pH 2.45, containing 12 percent acetonitrile and 10 mM heptofluorobutyric acid (HFBA) as an ion-pairing agent was trialled. 20 µl of sample or standard, dissolved in 1 percent HFBA were injected at a flow rate of 1 ml per minute. Under these conditions, the sample failed to elute after 30 minutes. The pH of the mobile phase was then lifted to 3.5 using weak sodium hydroxide, which resulted in the sample eluting with a single peak after approximately 3 minutes. To reduce significant peak tailing, 50 mM of ammonium formate was added to the solution, and the pH re-adjusted to 3.5 using formic acid. Finally, the acetonitrile concentration was progressively lowered until satisfactory separation of the pyridinoline and deoxypyridinoline peaks was achieved. The optimal acetonitrile concentration was found to be just 2 percent. Under these conditions, the retention times for pyridinoline and deoxypyridinoline were 3.4 minutes and 4.0 minutes respectively. While some peak tailing was still apparent, it was deemed sufficiently small such that it would be unlikely to significantly impact on the accuracy of results. The isocratic protocol developed was considered superior to many in the literature, due to its comparative speed and simplicity.

Prior to analyses, samples were purified according to the following procedure: 1 ml of sample was mixed with 1ml of glacial acetic acid and 200 µl of a stock slurry made from 5 g of microgranular cellulose, 66 ml of butanol, 17ml of acetic acid and 17 ml of deionised water, and vortexed. 4 ml of butanol were then added to each sample, and tubes were vortexed again. 4 ml of cellulose slurry were added to columns attached to a vacuum manifold. The cellulose was allowed to settle for 5 minutes, and

the liquid was then drained under vacuum. The samples were then poured onto the columns and drained. 7.5 ml of wash solution was added to the sample tubes, vortexed, and poured onto the columns and drained, then 7.5 ml of wash solution was added directly to the columns and drained. 0.5 ml tetrahydrofuran was then added to the columns, left to stand for 5 minutes, then drained. Finally, 1 ml of 1 percent HFBA was added to each column and vaccuum drained into a fresh set of sample tubes, which were centrifuged for 10 minutes at 4000 rpm. Samples were syringe filtered prior to injection.

5.5.3.2.4 Uronic Acid Assay

Uronic acid was measured using an established method (Blumenkrantz and Asboe-Hansen, 1973), adapted for use with a microplate reader. 50 µl aliquots of sample were combined with 150 µl of deionised water in glass test tubes. After cooling on ice, 1.2 ml of 0.0125 M sodium tetraborate in concentrated sulphuric acid was added to each tube, which were vortexed, covered and placed in boiling water for 5 minutes. Tubes were then placed back on ice, then, once cool, 200 µl of meta-hydroxydiphenyl solution (15 mg of 3-phenylphenol dissolved in 10 ml of 0.5 % sodium hydroxide) was added to each. After 5 minutes, 200 µl aliquots were transferred to the wells of a microplate, and absorbance was read at a wavelength of 520 nm. Serial dilutions of D-glucuronolactone and a blank (deionised water) were used to generate standard curves.

5.5.4 Results

5.5.4.1 Validation

5.5.4.1.1 Desmosine Assay

The standard curve for the desmosine assay is shown in Figure 5.6A. Each standard dilution was assayed in triplicate and averaged. Figure 5.6B shows the same standards plotted with a log scale on the horizontal axis.

For the four specimens evaluated in the preliminary study, the mean desmosine released into the extraction buffer by the elastase treatment was found to be 68.2 ± 15.4 percent (Table 5.5).

	Tissue			Extract			Tissue + Extract (μg)	Percent Extracted
	A490*	ng/ml	μg in total	A490*	ng/ml	μg in total		
Mean	1.935	5.79	1.16	1.768	12.44	2.49	3.65	68.2
SD	0.124	3.36	0.67	0.050	1.93	0.39	0.59	15.4

Table 5.5. Desmosine assay results (n = 4). *Absorbance measured at 490nm.

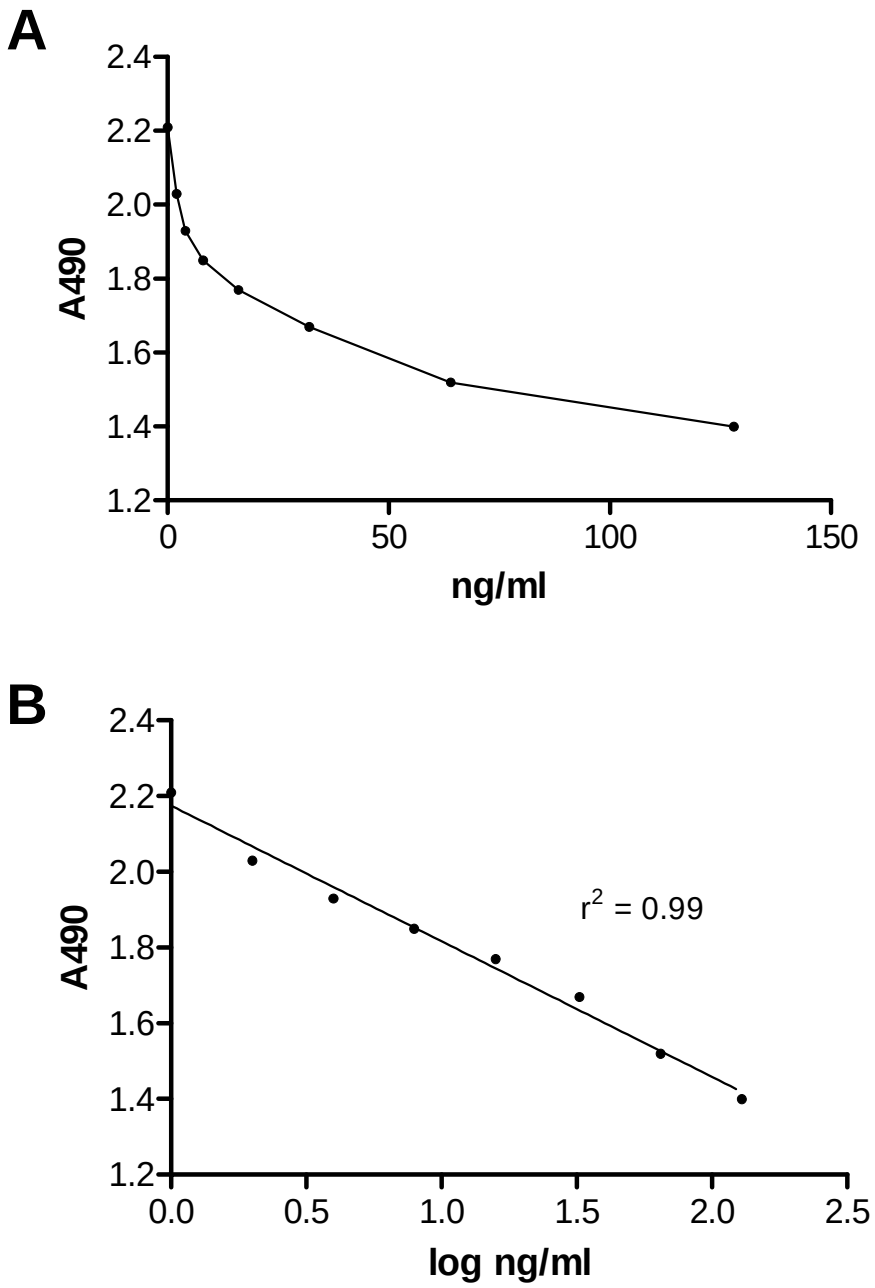


Figure 5.6. Standard curve for the desmosine assay. A. Linear scale horizontal axis. B. Logarithmic scale horizontal axis.

5.5.4.1.2 Hydroxyproline Assay

Figure 5.7 shows the standard curve for the hydroxyproline assay. For the four specimens evaluated in the preliminary study, the mean hydroxyproline released into the extraction buffer by the elastase treatment was found to be 4.6 ± 1.7 percent (Table 5.6).

	Tissue			Extract			Tissue + Extract (mg)	Percent Extracted
	A560*	µg/µl	mg in total	A560*	µg/µl	mg in total		
Mean	1.334	0.265	2.65	0.065	0.013	0.129	2.78	4.6
SD	0.152	0.030	0.30	0.017	0.003	0.036	0.29	1.7

Table 5.6. Hydroxyproline assay results (n = 4). *Absorbance measured at 560nm.

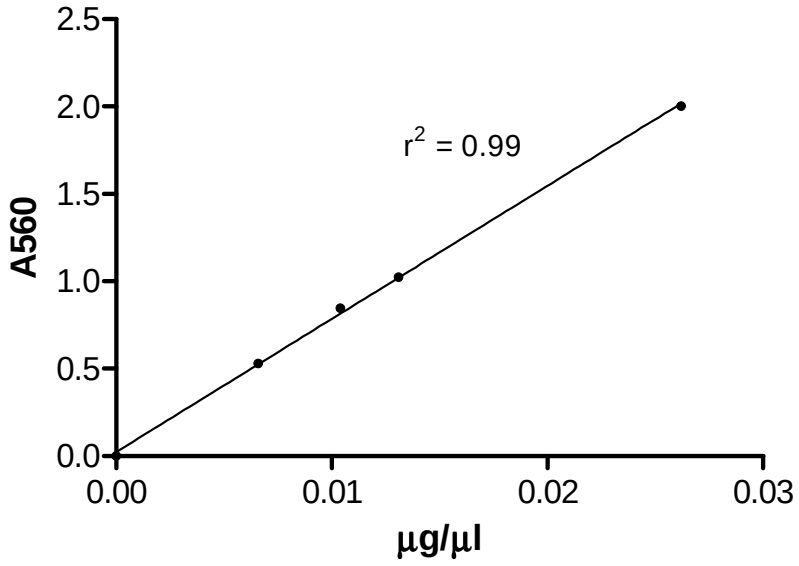


Figure 5.7. Standard curve for the hydroxyproline assay.

5.5.4.1.3 Pyridinoline Assay

Figure 5.8 shows the standard curve for the pyridinoline assay, and chromatographs of the serially diluted pyridinoline standards are illustrated in Figure 5.9 – the second, smaller peaks are deoxypyridinoline. For the four specimens evaluated in the preliminary study, the mean pyridinoline released into the extraction buffer by the elastase treatment was found to be 4.0 ± 1.9 percent (Table 5.7).

	Tissue			Extract			Tissue + Extract (nmol)	Percent Extracted
	Peak Area	nmol/ ml	nmol in total	Peak Area	nmol/ ml	nmol in total		
Mean	0.633	0.206	2.064	0.027	0.009	0.087	2.151	4.0
SD	0.192	0.064	0.640	0.008	0.003	0.025	0.626	1.9

Table 5.7. Pyridinoline assay results (n = 4).

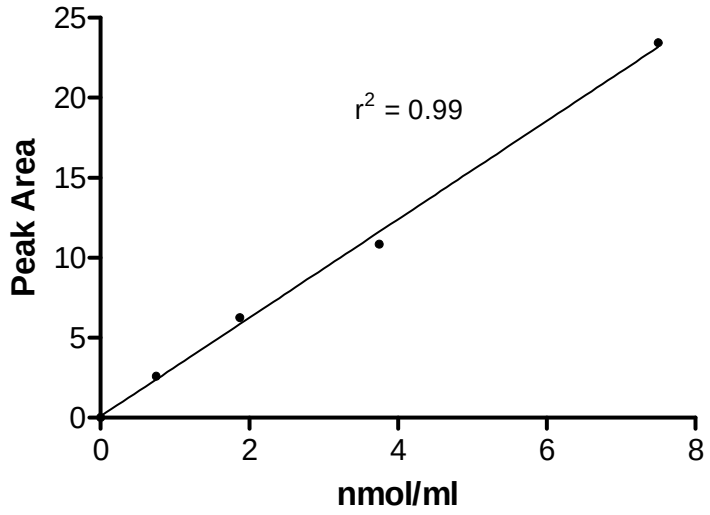


Figure 5.8. Standard curve for the pyridinoline assay.

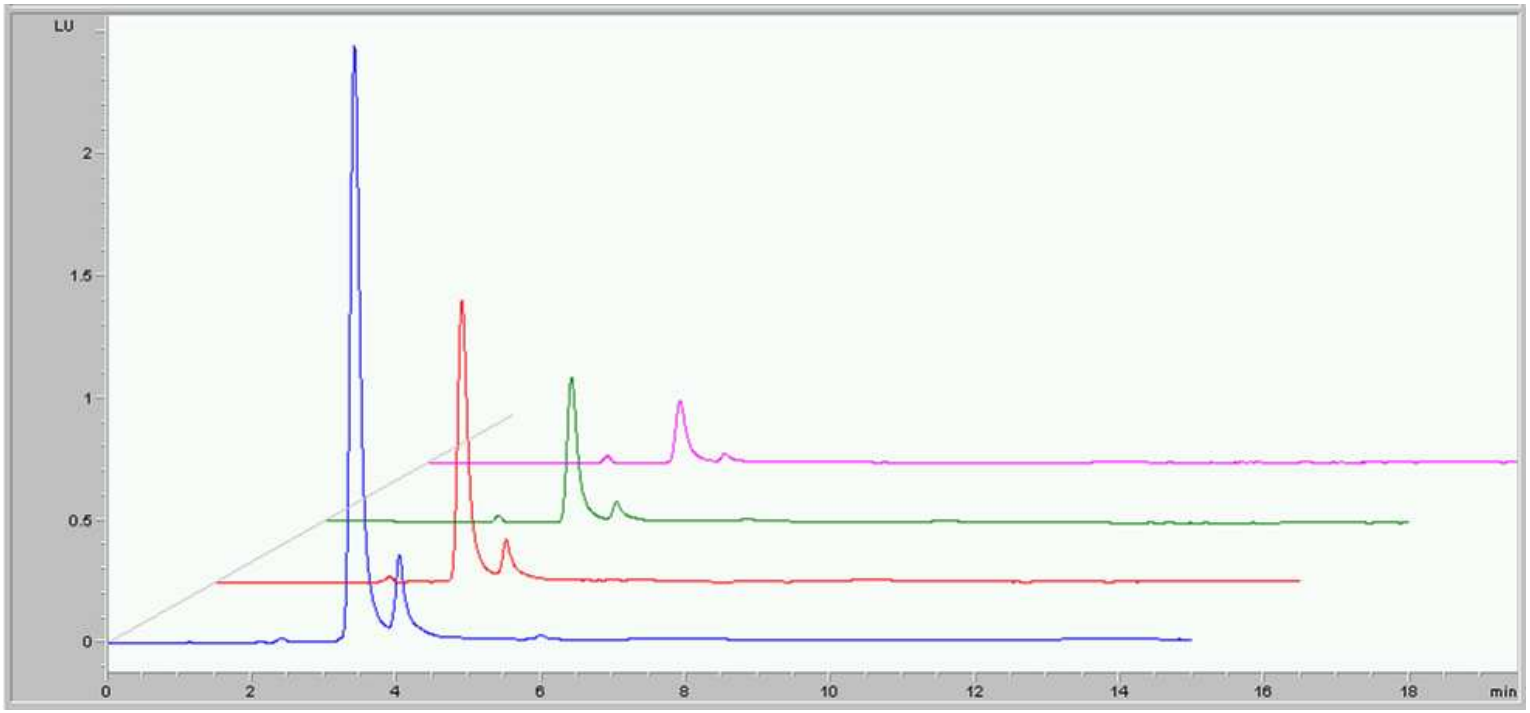


Figure 5.9. HPLC chromatographs for four serial dilutions of combined pyridinoline and deoxypyridinoline standard. The pyridinoline peak is at approximately 3.4 minutes.

5.5.4.1.4 Uronic Acid Assay

Figure 5.10 shows the standard curve for the uronic acid assay. For the four specimens subjected to the elastase treatment, the mean uronic acid released into the extraction buffer was 91.9 ± 1.7 percent (Table 5.8); for the four subjected to the chondroitinase ABC treatment, the mean extraction was 71.9 ± 4.7 percent (Table 5.9).

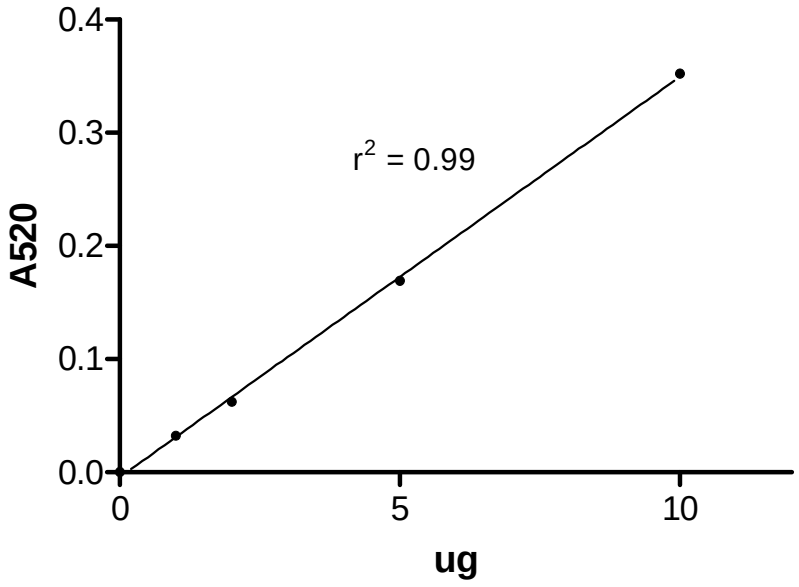


Figure 5.10. Standard curve for the uronic acid assay (assayed in triplicate, absorbance measured at 520nm).

	Tissue			Extract			Tissue + Extract (μg)	Percent Extracted
	A520*	**μg in 100μl**	**μg in total**	**A520***	**μg in 100μl**	**μg in total**		
Mean	0.091	2.36	47.28	0.584	26.77	535.40	582.67	91.9
SD	0.013	0.66	13.17	0.259	12.80	256.08	269.06	1.7

Table 5.8. Results of uronic acid assay for specimens subjected to elastase treatment. *Absorbance measured at a wavelength of 520nm.

	Tissue			Extract			Tissue + Extract (μg)	Percent Extracted
	A520*	**μg in 100μl**	**μg in total**	**A520***	**μg in 100μl**	**μg in total**		
Mean	0.149	5.22	104.46	0.313	13.35	267.08	371.54	71.9
SD	0.027	1.33	26.67	0.076	3.75	75.04	97.12	4.5

Table 5.9. Results of uronic acid assay for specimens subjected to chondroitinase ABC treatment. *Absorbance measured at a wavelength of 520nm.

5.5.5 Allocation of Specimens to Treatment Groups

Specimens from the anterolateral and posterolateral quadrants of the eight hemi-discs summarised in Table 5.1 were randomly assigned either to elastase or chondroitinase ABC digestion groups (descibed in section 5.5) using a random number table (Snedecor and Cochran, 1967). Assignments are detailed in Table 5.10.

Age-Quadrant-Number	Elastase	Chondroitinase ABC
16-AL-1		■
16-AL-2	■	
16-PL-1	■	
16-PL-2		■
28-AL-1		■
28-AL-2	■	
28-PL-1		■
28-PL-2	■	
40-AL-1	■	
40-AL-2		■
40-PL-1		■
40-PL-2	■	
57-AL-1		■
57-AL-2	■	
57-PL-1	■	
57-PL-2		■
66-AL-1		■
66-AL-2	■	
66-PL-1	■	
66-PL-2		■
76-AL-1		■
76-AL-2	■	
76-PL-1	■	
76-PL-2		■
80-AL-1	■	
80-AL-2		■
80-PL-1	■	
80-PL-2		■
87-AL-1	■	
87-AL-2		■
87-PL-1		■
87-PL-2	■	

Table 5.10. Specimen assignments to digestion groups.

5.5.6 Discussion

The results of the desmosine immunoassay demonstrated that the elastase treatment degraded the majority of the elastic fibres in the matrix. As noted in a previous study, desmosine is a tetrafunctional crosslink, meaning that elastin must be cleaved at four separate sites around the crosslinks for them to be solubilised (Lee *et al.*, 2001). This suggests that, although crosslink solubilisation was not complete as measured by the assay, functional compromisation of elastic fibres may have in reality been more comprehensive.

Hydroxyproline and pyridinoline assays demonstrated that the elastase treatment had only a small degradative effect on collagen. This occurred despite inclusion of the soybean trypsin inhibitor, and therefore appeared unavoidable. A previous study using similar techniques reported no effect on the mechanical properties of pure collagen, despite some minor biochemical changes (Missirlis, 1977). This minor collagen loss was thus considered acceptable for the purposes of this study. Interestingly, the degrees of hydroxyproline degradation and pyridinoline degradation were highly correlated, suggesting that any degradation that did occur was uniform in terms of both the triple-helical region of the collagen molecules and their mature enzymatic crosslinks.

Uronic acid assays demonstrated that both treatments resulted in the majority of glycosaminoglycans being lost from the matrix. While chondroitinase ABC treatments were used to account for mechanical changes which occurred due to non-specific glycosaminoglycan degradation by elastase, this enzyme does not specifically degrade keratan sulphate, which constitutes a significant proportion of anulus glycosaminoglycans (Eyre, 1979). Additionally, the uronic acid assay used did not

account for any such losses by either treatment, as keratan sulphate does not contain uronic acid chains (Yoon and Halper, 2005). Any speculative changes in mechanical properties resulting from non-specific degradation of keratan sulphate by the elastase treatment would therefore not be reflected in the changes associated with the chondroitinase ABC treatment.

5.6 Mechanical Testing

5.6.1 Review of Techniques

Isolated specimens of human anulus fibrosus have been tested extensively in uniaxial tension to determine their quasi-static mechanical properties. Mechanical testing of soft tissues more generally poses a number of practical challenges, more so when specimens are comparatively small and delicate. In this section, techniques used to overcome the most critical of these challenges are reviewed and evaluated.

Gripping of Specimens: The size, shape and texture of excised anulus fibrosus specimens presents difficulties when it comes to mounting them in the grips of a mechanical testing system. Methods used previously range from using serrated grips (Wu and Yao, 1976), lining the grips with polishing paper (Skaggs *et al.*, 1994; Acaroglu *et al.*, 1995; Ebara *et al.*, 1996), pre-mounting specimens in rigid sand-paper frames (Fujita *et al.*, 1997), using cyanoacrylate adhesives (Wu and Yao, 1976; Fujita *et al.*, 1997), gripping stainless steel wire rods inserted into each end of the specimen (Wagner and Lotz, 2004), and gripping suture, sewn and knotted into each end of the specimen (Wagner *et al.*, 2006). Whatever the gripping method, preventing specimen slippage is critical. Based on the specimen sizes and profiles proposed for this study, rigid, disposable sandpaper frames were considered the best option. The rigidity of these frames enables specimens to be transferred to the grips of the test system while maintaining a fixed gauge length and limiting distortion, before the frames sides are cut to enable testing. The use of polystyrene spacers attached to each corner of the frame is an established means for evenly distributing the force of the grips across the specimen ends and preventing crushing (Fujita *et al.*, 1997). These spacers were therefore also included in this study. Cyanocrylate adhesive was not used, as it would

have compromised the ability to demount specimens, apply enzymatic treatments and repeat testing. Preliminary trials indicated slippage did not occur during the application of non-destructive strains.

Environmental Conditions: The maintenance of stable specimen hydration levels during mechanical testing is essential. Techniques used previously range from testing in air, with and without controlled humidity (Galante, 1967; Wu and Yao, 1976; Marchand and Ahmed, 1989), to testing in a saline bath (Skaggs *et al.*, 1994; Acaroglu *et al.*, 1995; Ebara *et al.*, 1996; Fujita *et al.*, 1997; Fujita *et al.*, 2000; Elliott and Setton, 2001; Holzapfel *et al.*, 2004; Iatridis *et al.*, 2005). Testing in a saline bath is the most common and effective method of maintaining a constant level of hydration for the duration of the test. In this study, the potential for variations in tissue hydration was of concern, and thus testing in a bath was considered the most appropriate technique. It was recognised that potential hyperswelling may result in mechanical properties which differ form those which exist in vivo; however, the comparative nature of proposed assessments (before and after treatments, between regions and between non-degenerate and degenerate specimens) meant this fact would be unlikely to adversely impact results. Additionally, testing in the bath enabled pre-treatment mechanical properties to be compared effectively with those determined in previous studies conducted under similar conditions.

Gauge Region Definition: For uniaxial mechanical tests it is common to use dumb-bell shaped specimens (those with a reduced central gauge region) so that stresses are concentrated and failure is promoted within a defined region, distant from the grip-tissue interfaces. Numerous studies of the anulus fibrosus have used dumbbell shaped specimens for this reason (Wu and Yao, 1976; Skaggs *et al.*, 1994; Acaroglu *et al.*,

1995; Ebara *et al.*, 1996). Other studies have opted for parallel-edged specimens where the length of the gauge region is defined by the grip distance or markers on the tissue surface between the grips (Fujita *et al.*, 1997; Elliott and Setton, 2001; Holzapfel *et al.*, 2004; Iatridis *et al.*, 2005; Wagner *et al.*, 2006). This second method is often selected where there are limitations associated with the small size of the specimens. While in this study incorporating a reduced central gauge region was considered the best option, preliminary trials indicated that the specimens were prohibitively small. Parallel-edged specimens were therefore used, with the gauge region defined as the distance between the grip interfaces.

Strain Measurement: Strain measurement techniques applied previously in the mechanical testing of anulus fibrosus specimens broadly fall into two categories: measurement of grip travel using, for example, a linear variable differential transformer (LVDT) (Fujita *et al.*, 1997; Iatridis *et al.*, 2005), or non-contact measurement of strain either in terms of grip travel, artificial marks on the tissue surface such as ink, plastic or pins (Skaggs *et al.*, 1994; Acaroglu *et al.*, 1995; Ebara *et al.*, 1996; Holzapfel *et al.*, 2004; Wagner and Lotz, 2004; Wagner *et al.*, 2006), or aspects of pre-existing tissue architecture or colouration (Elliott and Setton, 2001). In this study, given the practicalities associated with size of the specimens and gauge regions, grip-travel as measured by the high resolution displacement transducer on the mechanical testing system (described in section 5.6.2.2) was considered the best possible method of strain measurement.

Preconditioning: When a cyclic loading regime is applied to soft tissue specimens, the load versus deformation curve is observed to shift to the right, and the hysteresis loop size to progressively decrease, with each subsequent cycle. After a definite number of

cycles, the shift of the curve and change in hysteresis loop size subside and the specimens is said to be preconditioned (Fung, 1981). Precondtioning is therefore essential for obtaining repeatable results. It is believed to occur due to the progressive realignment of structural elements within the tissue, and the expulsion and redistribution of interstitial fluid (Fung, 1981). Most previous investigations of anulus tissue-level mechanical behaviour have initially applied a preconditioning regime. The number of cycles to reach a steady state response in these studies varies from five (Fujita *et al.*, 1997), to eight (Elliott and Setton, 2001) to ten (Skaggs *et al.*, 1994; Acaroglu *et al.*, 1995; Ebara *et al.*, 1996), indicating possible dependance on specimen size, shape or orientation. For this study, it was therefore resolved to determine the optimum number of cycles experimentally.

Strain Rate Dependence: There is evidence that mechanical response of soft tissues tested in vitro exhibits strain rate dependence (Fung, 1981). Tissues with both a solid and a fluid phase may demonstrate higher elastic modulus when strain rates exceed the maximum flow rate of the fluid phase. With respect to the anulus fibrosus, hysteresis energy loss and toe region modulus for axially oriented specimens following preconditioning have been shown to exhibit significant strain rate dependence (Kasra *et al.*, 2004). In contrast, the quasi-static mechanical properties of radially oriented specimens were found to be independent of strain rate across the range 0.005 to 50 percent per second (Fujita *et al.*, 1997). Strain rates of 0.5 percent per second (Fujita *et al.*, 1997) and 0.01 percent per second (Elliott and Setton, 2001) have been used previous for quasi-static ramp tests of radially oriented specimens, and have produced comparable results for initial modulus and ultimate modulus, providing further evidence of strain rate independence. A strain rate of 0.25 percent per second,

corresponding with the lower limit of the capabilities of the mechanical testing system was adopted for this study, and considered appropriate in the context of previous investigations.

Engineering Stress or True Stress: Engineering stress is defined as the instantaneous force divided by the undeformed (initial) cross-sectional area of the specimen, where as true stress is defined as the instantaneous force divided by the instantaneous 'deformed' cross-sectional area (Askeland, 1996). To calculate deformed true stress, therefore, it is necessary to monitor strains in all 3 dimensions (length, width and thickness). Many studies use engineering stress, based on the assumption that the soft tissues are intrinsically incompressible due to high water content (Humphrey, 2003). There are also technical difficulties associated with measuring strains on multiple surfaces. The assumption of incompressibility was made with respect to specimens due to their high water content following saline equilibration, although the validity of this assumption was not made experimentally. For this reason, and due to the impracticallities associated with measuring strains in all three dimensions and to permit valid comparisons with the results of previous studies, it was resolved to use engineering stress.

5.6.2 Methods

5.6.2.1 Specimen Mounting

To facilitate precise mounting of specimens in the grips of the testing machine, custom frames were constructed for each specimen from 150 grit silicon carbide polishing paper. Polystyrene spacers were glued to the corners of each frame to ensure the gripping force was evenly distributed over the surface of the specimen ends, and to prevent crushing. The gauge region, defined as the frame window height, was measured using ± 0.01 mm resolution digital calipers to be 2.19 ± 0.11 mm. Frames with equivalent gauge region dimensions (± 0.05 mm) were paired for each specimen, for pre- and post-treatment tests.

Specimens were thawed at room temperature and re-equilibrated for 1 hour in 0.15 M phosphate buffered saline at 4°C, then mounted in a sandpaper frame as shown disassembled in Figure 5.11. To facilitate gauge region relocation for re-testing following treatment, the location of the frame window relative to aspects of specimen macro-architecture was qualitatively assessed and indicated on the high resolution digital image originally used for measuring dimensions. The two sides of the frame were then pressed together and fixed using fast drying adhesive, and the complete unit transferred to the grips of the mechanical testing system. Prior to testing, the sides of the frame were carefully cut using a number 15 blade scalpel, and the grips submerged in an bath containing 0.15 M phosphate buffered saline, pH 7.4 at room temperature.

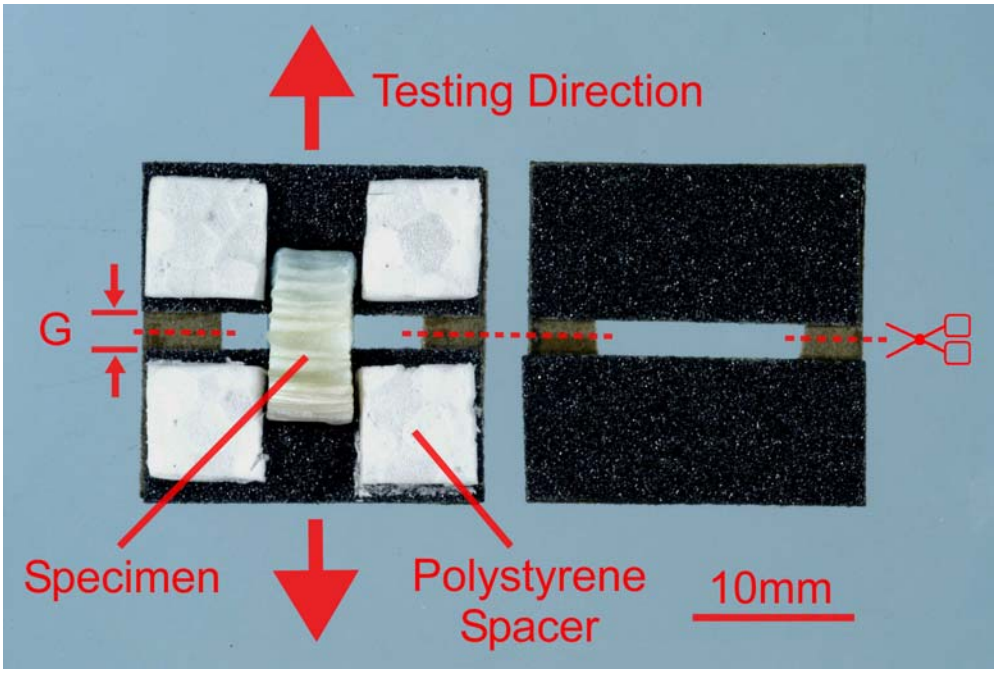


Figure 5.11. Sandpaper mounting frame (prior to assembly) with specimen in position. G = gauge region; dotted lines = cutting zones following placement in the mechancial testing system grips.

5.6.2.2 Mechanical Testing System Description

The mechanical testing system used in this study was a Mach-1 A400.25 (Biosyntech, Laval, Canada), (Figure 5.12). Figure 5.13 shows a closer view with the test rig including grips submerged in saline. The system incorporated a load cell with a resolution of 0.005 N, and a LVDT with a displacement resolution of 0.05 μm. The system was controlled via a computer running Mach-1 Motion software (Biosyntech, Laval, Canada), which displayed load versus displacement data in real time during testing.



Figure 5.12. Biosyntech Mach-1 mechanical testing system.

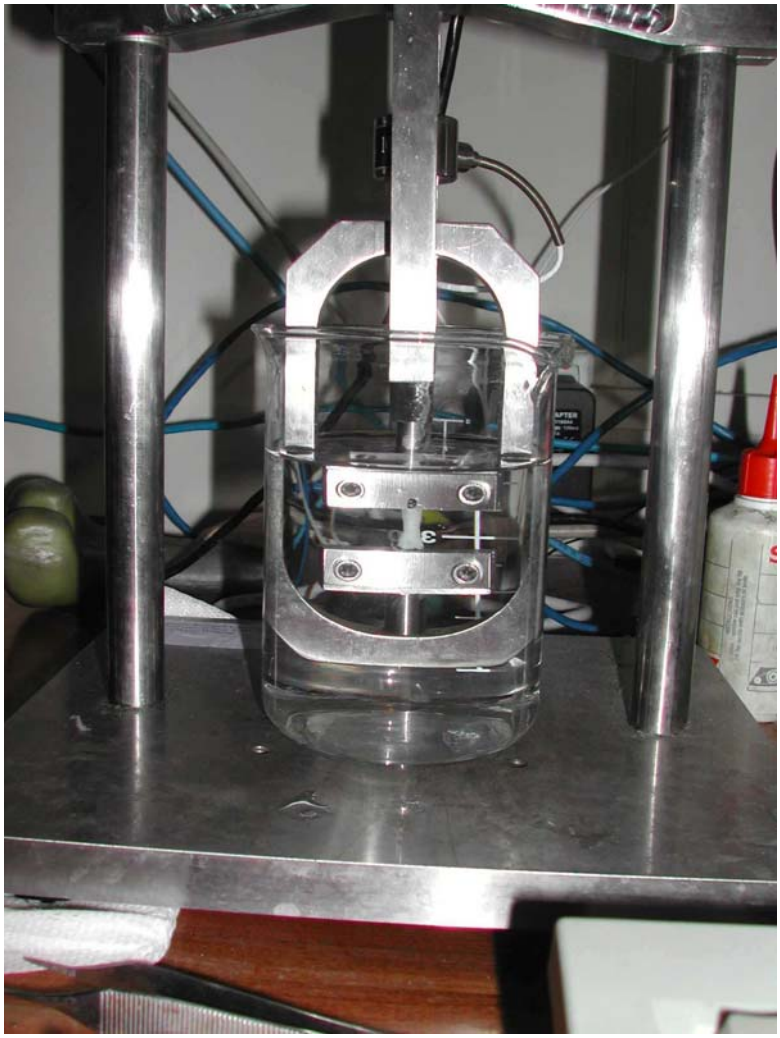


Figure 5.13. Specimen under test submerged in saline.

5.6.2.3 Determination of Maximum Strain

It was critical that the maximum strain amplitude used for quasi-static tests exceed the extensibility of specimens to permit determination of ultimate modulus, but significantly precede the yield strain to enable repeat testing. Previous studies and preliminary work suggested that these properties vary considerably with region and condition, as well as before and after enzymatic treatment (Fujita *et al.*, 1997). The optimum maximum strain amplitudes were therefore determined experimentally for each specimen immediately prior to preconditioning, by applying a constant strain rate ramp at 5 percent per second until the response was observed to significantly exceed the transition strain into the second linear region. Maximum strain amplitudes (mean ± SD) were 0.31 ± 0.11 mm/mm for pre-treatment tests, and 0.46 ± 0.19 mm/mm and 1.22 ± 0.50 mm/mm following chondroitase ABC and elastase treatments respectively. Both preconditioning and subsequent quasistatic ramp tests were conducted to these strains.

5.6.2.4 Preconditioning

Specimens were initially allowed to equilibrate for five minutes under a small preload of approximately 0.01 N. Five cycles of preconditioning using a triangular waveform were then applied at a strain rate corresponding to approximately 5 percent per second under displacement control, between zero strain and a maximum strain determined as described in section 5.6.2.3, after which the response was observed to be repeatable.

5.6.2.5 Quasi-Static Testing

Following preconditioning, an incremental displacement was then manually introduced until the system just registered tension. The magnitude of this incremental

displacement was recorded, and combined with the original sandpaper frame window height to define the initial gauge length. A single ramp test to the same maximum strain as used for preconditioning was conducted under displacement control at a velocity of 5 μm per second, corresponding to a strain rate of approximately 0.25 percent per second. This was the minimum displacement velocity obtainable with the system. The preconditioning and quasi-static testing protocols were repeated for each specimen following enzymatic treatment. Data were acquired at a rate of 10 Hz.

5.6.2.6 Repeatability

The repeatibility of the mechanical tests was tested in a preliminary study. Four specimens, separate from those allocated to the primary treatment groups but prepared using the same protocol, were tested non-destructively using the methods outlined. They were then removed from the clamps and re-equilibrated in phosphate buffered saline for approximately one hour, considered sufficiently long for solid and fluid tissue constituents to return to their pre-test homeostatic configuration, but sufficiently short to prevent significant loss of glycaosminoglycans through ionic diffusion, then retested using the same protocol. Initial modulus, ultimate modulus and extensibility were compare for the initial and repeat tests using paired Student's t-tests, and any significant differences reported for two-tailed p values less than 0.05.

5.6.2.7 Analysis

Engineering stress (force divided by undeformed cross-sectional area at equilibrium hydration) vs strain (the instantaneous length divided by the starting length) was plotted for each specimen before and after treatment. Initial modulus, ultimate modulus and extensibility (Figure 1.7) were calculated from the raw data. Previous

studies of anulus tensile mechanical properties have defined elastic modulus either as the tangent to the linear region of the curve at a prescribed percentage of the yield strain, or using moving cell linear regression, in which the regression line with the optimum coefficent of determination defines the modulus (Ebara *et al.*, 1996; Fujita *et al.*, 1997). As the testing in this study was non-destructive, the second of these methods was adopted. For ultimate modulus, regression commenced at the maximum strain; for initial modulus, the regression started at zero strain. Extensibility was defined as the transition strain between the initial linear and ultimate linear regions of the curve, and calculated as the intersection point of tangents to these to regions.

5.6.2.8 Statistics

Statistic analyses were performed using GraphPad Prism V5 (GraphPad Software Inc., San Diego, CA, USA). Paired mechanical testing data sets, before and after treatments, were assessed separately for normality using the Shapiro-Wilk test. Statistical differences for each property (initial modulus, ultimate modulus and extensibility) between pre-treatment and post-treatment measurements were assessed using paired Student's t-tests where data were normally distributed (expressed as mean ± standard deviation (SD)), or using the Wilcoxon signed ranks test where data were non-parametric (expressed as median, interquartile range (IQR)). Student's t-test or a Mann-Whitney U test were used to compare the effect of region (anterolateral vs posteralateral), and the effect of degeneration (specimens grouped as grade 1or 2 versus grade 3 or 4) on mechanical properties. Significance was reported for 2-tailed p values less than 0.05.

5.6.3 Results

5.6.3.1 Repeatability

Untreated specimens subjected to repeat testing following one hour of re-equilibration displayed no significant change in initial modulus (initial test: 0.11 ± 0.07 MPa, repeat test: 0.10 ± 0.07 MPa, $p = 0.4$, mean ± SD), ultimate modulus (initial test: 0.21 ± 0.10 MPa, repeat test: 0.23 ± 0.10 MPa, $p = 0.6$) or extensibility (initial test: 0.26 ± 0.11 mm/mm, repeat test: 0.29 ± 0.12 MPa, $p = 0.2$).

5.6.3.2 Cross-Sectional Area

Following enzyme treatments, specimen dimensions were remeasured. Specimens treated with elastase or chondroitinase ABC each displayed a significant decrease in cross-sectional area (elastase treated: 17 percent, $p = 0.004$; chondroitinase ABC treated: 10 percent, $p = 0.03$). As a result, post-treatment cross-sectional areas were used in stress calculations for post-treatment mechanical testing results, for both treatment groups.

5.6.3.3 Initial Length

Following treatment with elastase, specimen initial length increased significantly by 14 percent compared with the pre-treatment value ($p = 0.008$). In contrast, specimens treated with chondroitinase ABC exhibited a significant decrease in initial length of 9 percent compared with the pre-treatment value ($p = 0.03$).

5.6.3.4 Mechanical Properties

Typical stress-strain responses before and after each of the treatments are illustrated in Figure 5.14.

5.6.3.4.1 Initial Modulus

The median pre-treatment initial modulus for all specimens was 0.077 (0.036,0.106) MPa (median (IQR)). Pre-treatment and post-treatment initial modulus results for elastase and chondroitinase ABC treated specimens are illustrated in Figure 5.15 and Figure 5.16 respectively. For those treated with elastase, initial modulus decreased significantly ($p < 0.001$). Those treated with chondroitinase ABC also displayed a significantly decreased initial modulus ($p < 0.001$). The magnitude of the decrease experienced by those treated with elastase was significantly greater than that experienced by those treated with chondroitinase ABC ($p < 0.001$) (Figure 5.17).

5.6.3.4.2 Ultimate Modulus

The mean pre-treatment ultimate modulus for all specimens was 0.211 (0.109,0.266) MPa (median (IQR)). Pre- and post-treatment ultimate modulus values for elastase and chondroitinase ABC treated specimens are illustrated in Figure 5.15 and Figure 5.16 respectively. For those treated with elastase, ultimate modulus decreased significantly ($p < 0.001$). Those treated with chondroitinase ABC displayed no significant change in ultimate modulus ($p = 0.86$). Post-treatment ultimate modulus for chondroitinase ABC treated specimens was therefore excluded from region and condition comparisons.

5.6.3.4.3 Extensibility

The mean pre-treatment extensibility for all specimens was 0.160 (0.136,0.188) mm/mm (median (IQR)). Pre- and post-treatment extensibility values for elastase and chondroitinase ABC treated specimens are are illustrated in Figure 5.15 and Figure 5.16 respectively. For those treated with elastase, extensibility increased significantly ($p < 0.001$). Those treated with with chondroitinase ABC also displayed a significant, but smaller increase ($p < 0.001$). The magnitude of the decrease experienced by those treated with elastase was significantly greater than that experienced by those treated with chondroitinase ABC ($p < 0.001$) (Figure 5.17).

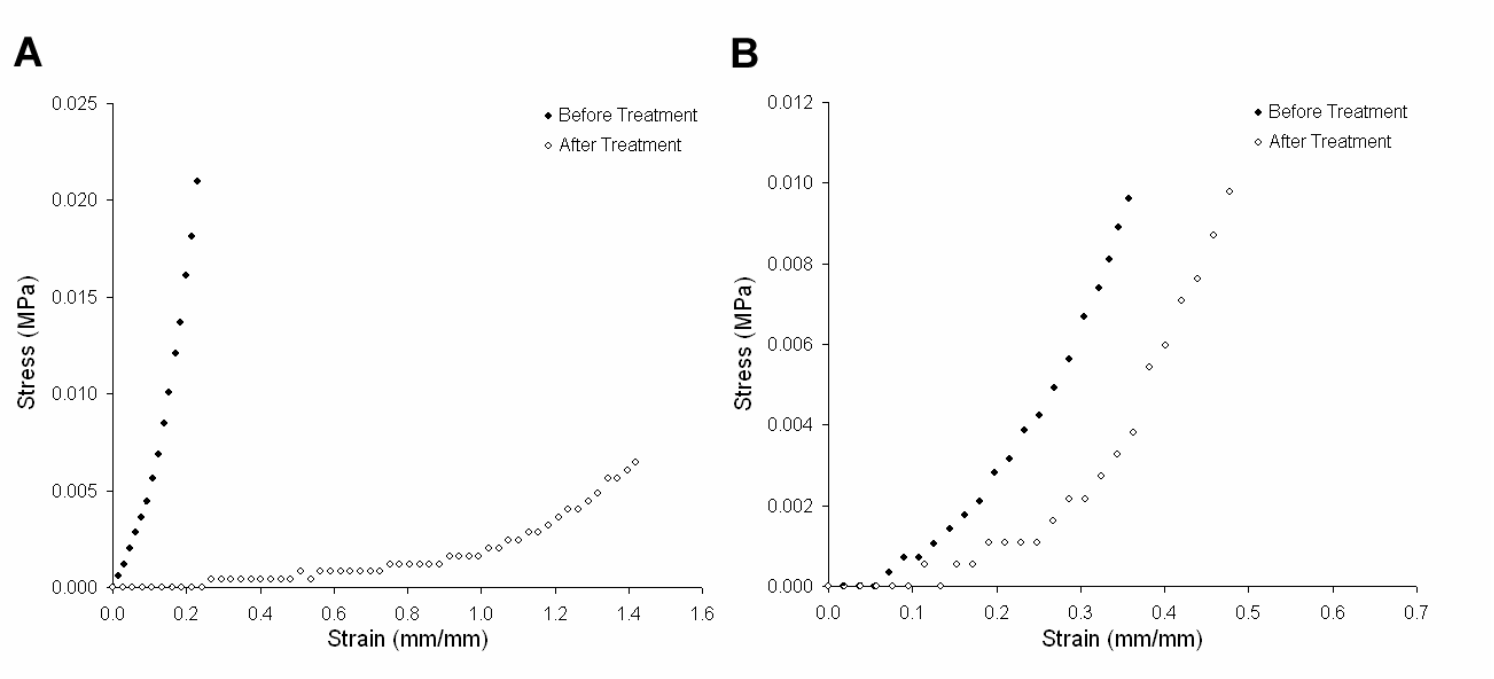


Figure 5.14. Typical stress versus strain responses A. before and after elastase treatment, and B. before and after chondroitinase ABC treatment.

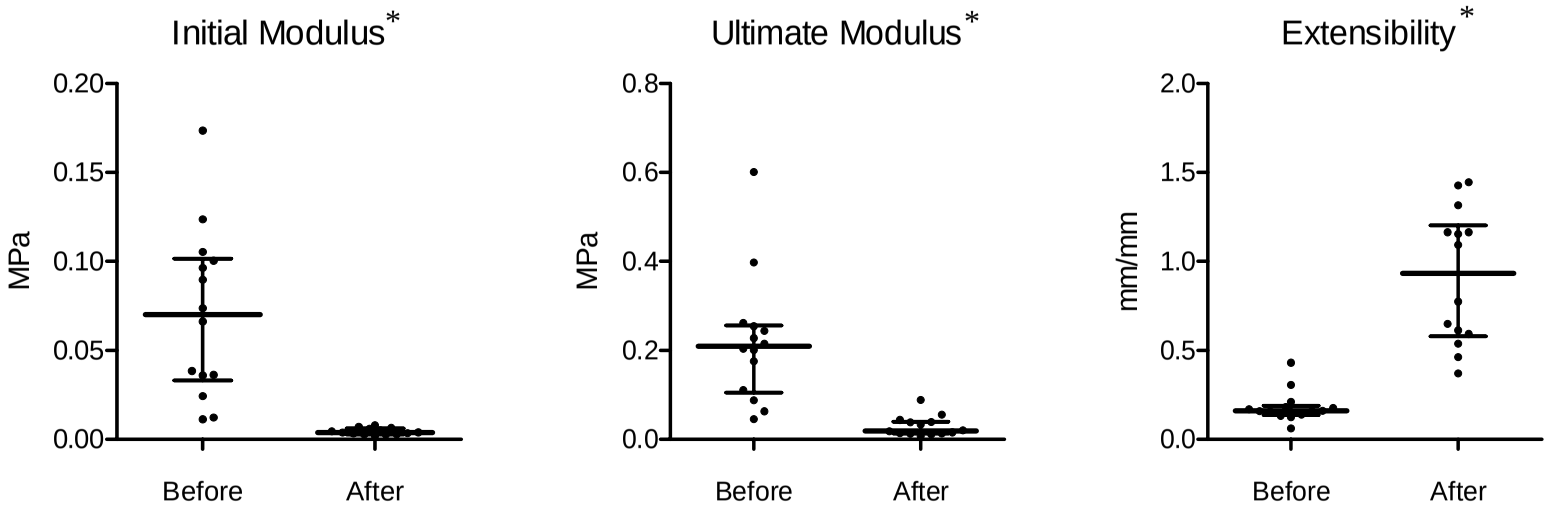


Figure 5.15. Initial modulus, ultimate modulus and extensibility, before and after elastase treatment (n = 14; all median + IQR). * Indicates significant difference between median values before and after treatment, $p < 0.001$.

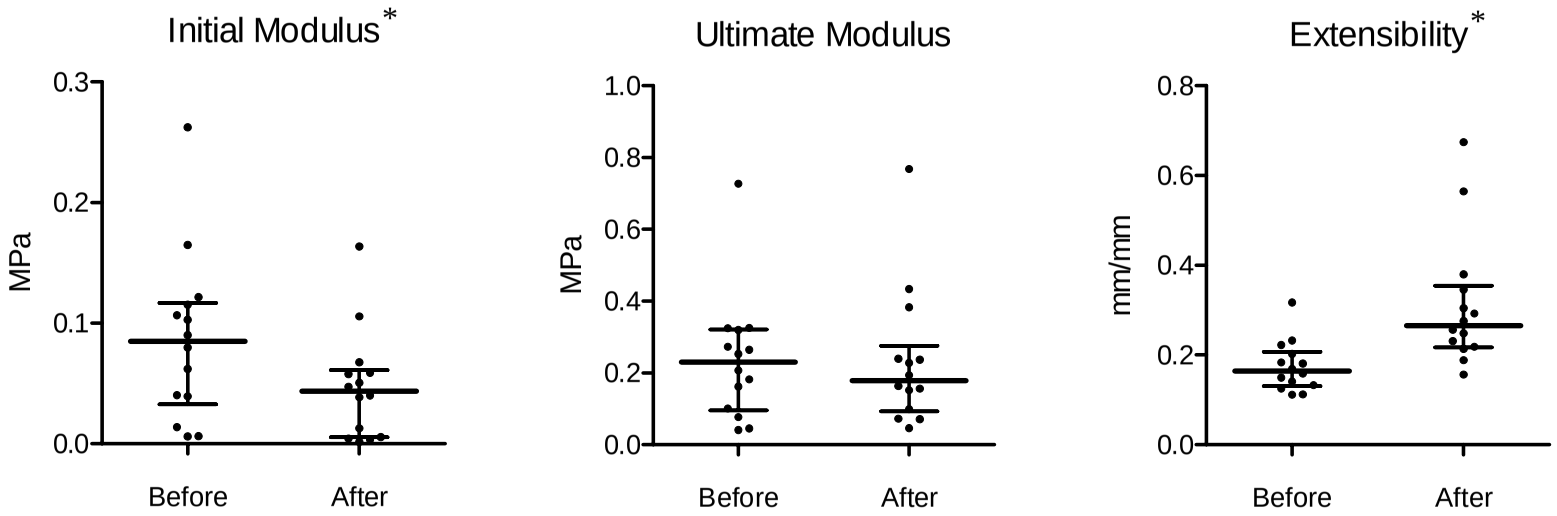


Figure 5.16. Initial modulus, ultimate modulus and extensibility, before and after chondroitinase ABC treatment. (n = 14; all median + IQR). * Indicates significant difference before and after treatment, $p < 0.001$.

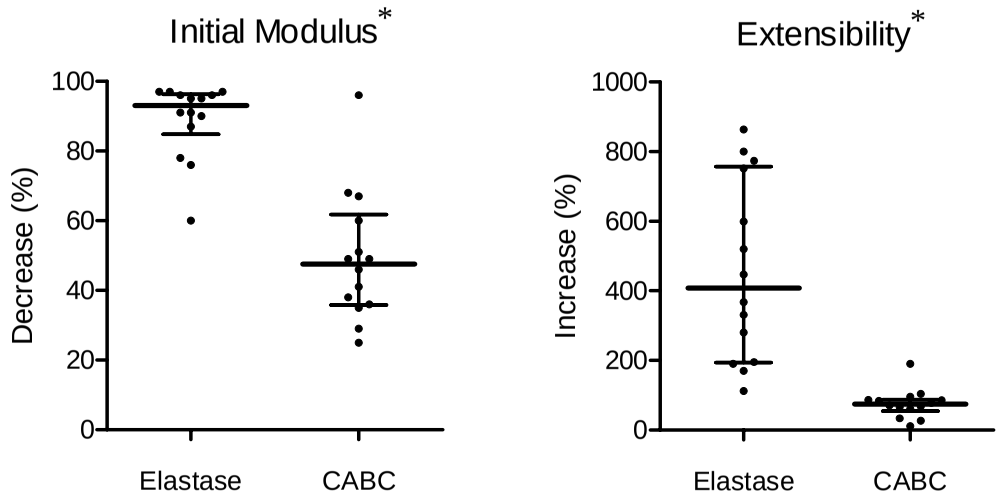


Figure 5.17. Comparison of the changes in initial modulus and extensibility following treatment with elastase and chondroitinase ABC (n = 14; median + IQR). * Indicates significant difference, $p < 0.001$.

5.6.3.5 Effects of Region

Comparisons of pre-treatment results between specimens from anterolateral and posterolateral quadrants are illustrated in Figure 5.18. Initial modulus and ultimate modulus were found not to be significantly different between anterolateral and posterolateral quadrants ($p = 0.11$ and $p = 0.17$ repectively), although trends were observed for both in which posterolateral specimens had a smaller values than anterolateral specimens. Extensibility was found to be significantly greater in specimens from posterolateral quadrants ($p = 0.02$).

Regional variations in mechanical properties following elastase treatment are illustrated in Figure 5.19. Differences in initial and ultimate elastic modulus between anterolateral and posterolateral specimens continued to be insignificant ($p = 0.55$ and $p = 0.16$ repectively). Extensibility, however, remained significantly greater for posterolateral specimens than anterolateral specimens ($p = 0.02$).

Regional variations in mechanical properties after chondroitinase ABC treatment are illustrated in Figure 5.20. Following chondroitinase ABC treatment, neither initial modulus nor extensibility were significantly different between anterolateral and posterolateral specimens ($p = 0.08$ and $p = 0.11$ respectively). Ultimate modulus was excluded from the comparison as it was statistically unaffected by the chondroitinase ABC treatment.

Regional variations in the magnitude of the change in mechanical properties after elastase treatment are illustrated in Figure 5.21. Neither the magnitude of the changes in initial or ultimate modulus were significantly different between anterolateral and

posterolateral quadrants ($p = 0.56$ and $p = 0.46$ respectively), nor did the magnitude of the change in extensibility ($p = 0.45$).

Regional variations in the magnitude of the change in mechanical properties after chondroitinase ABC treatment are illustrated in Figure 5.22. Neither the magnitude of the change in initial modulus or extensibility were significantly different between anterolateral and posterolateral specimens ($p = 0.18$ and $p = 0.79$ respectively.

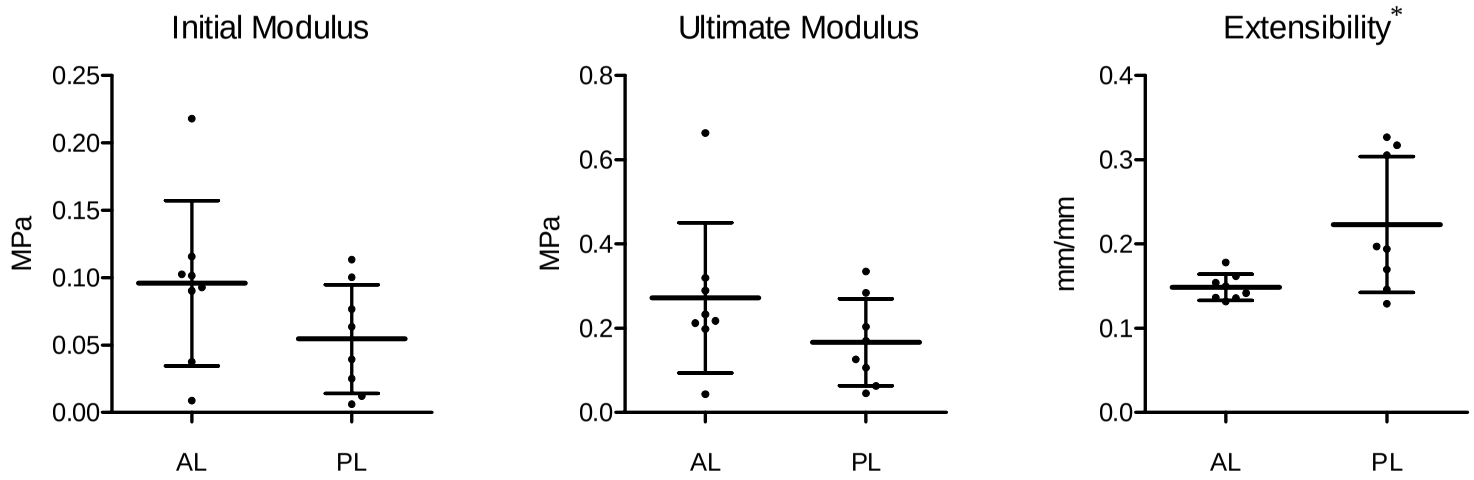


Figure 5.18. Variations in pre-treatment mechanical properties with circumferential location. (AL: n = 8; PL: n = 8; all mean ± SD). * Indicates significant difference between anterolateral and posterolateral, p = 0.02.

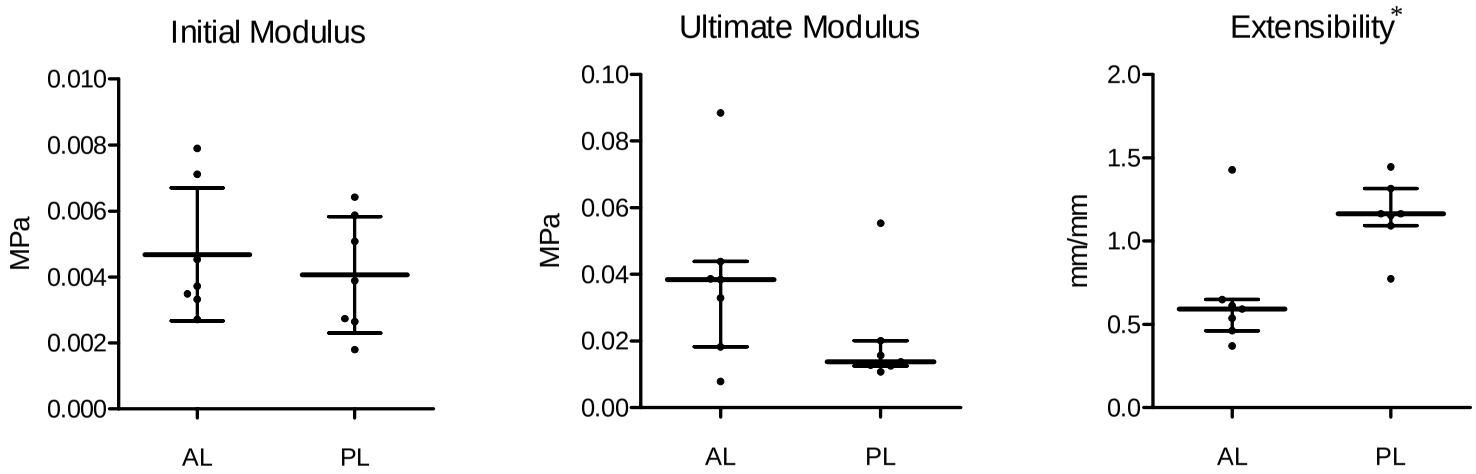


Figure 5.19. Variations in mechanical properties with circumferential location following treatment with elastase (AL: n = 7; PL: n = 7; initial modulus: mean ± SD; ultimate modulus and extensibility: median + IQR). * Indicates significant difference between anterolateral and posterolateral, p = 0.02.

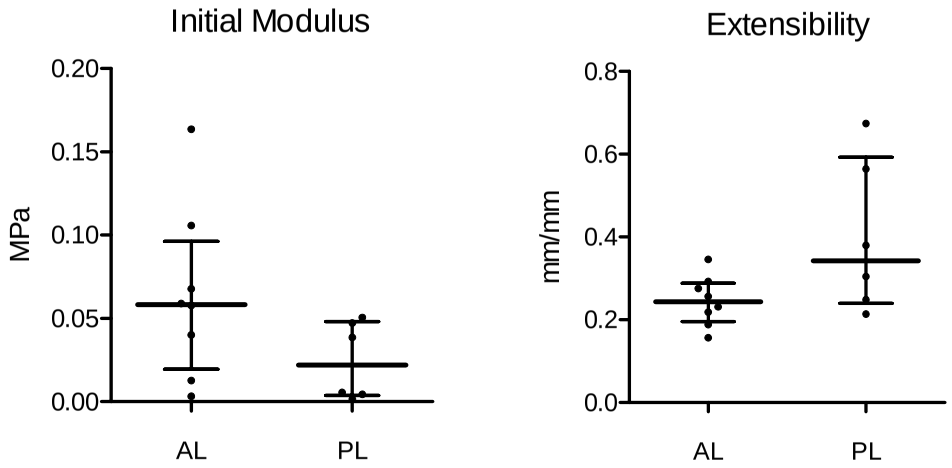


Figure 5.20. Variations in mechanical properties with circumferential location following treatment with chondroitinase ABC (AL: n = 8; PL: n = 6; both median + IQR).

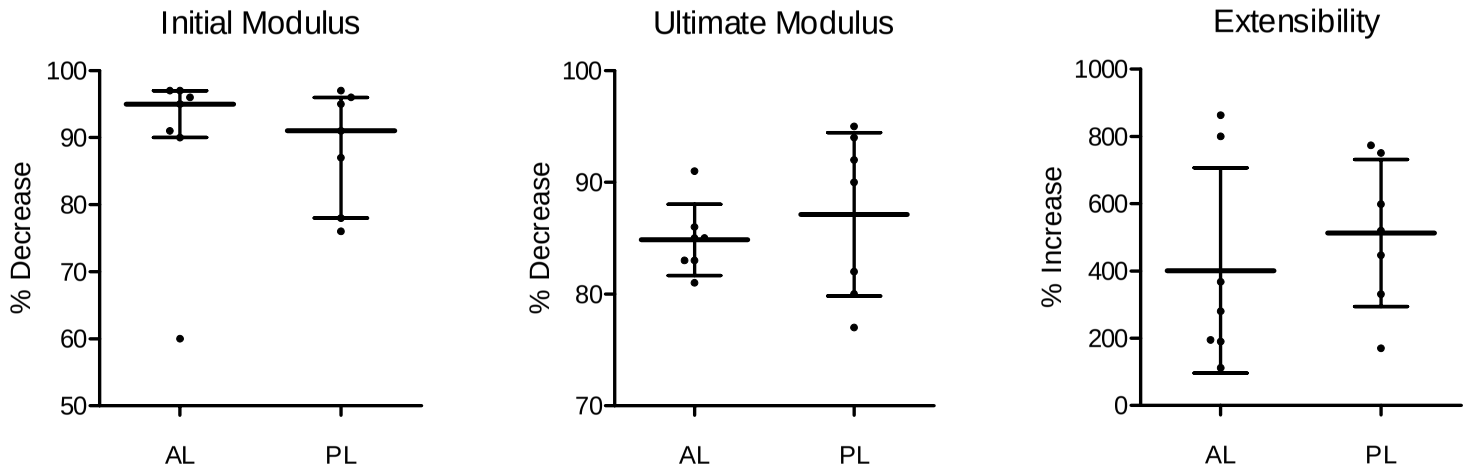


Figure 5.21. Variations in the magnitude of the changes associated with each of the mechanical properties with circumferential region following treatment with elastase (AL: n = 7; PL: n = 7; initial modulus: median + IQR; ultimate modulus and extensibility: mean ± SD).

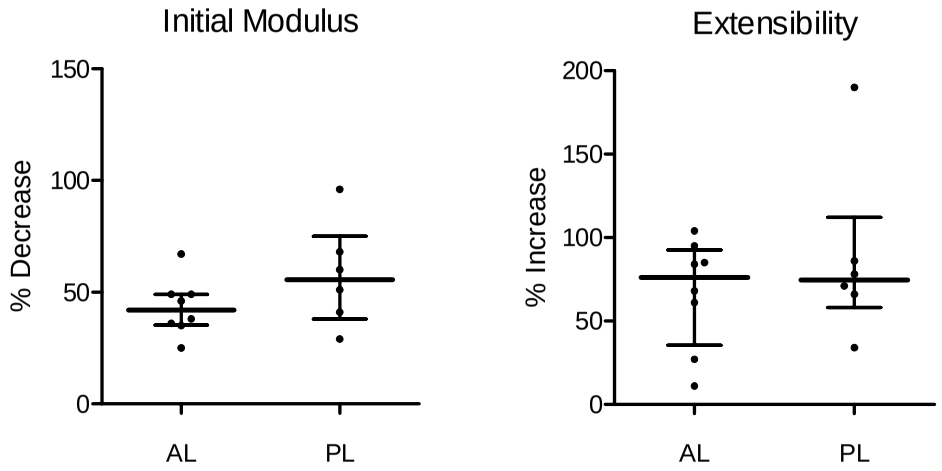


Figure 5.22. Variations in the magnitude of the changes associated with each of the mechanical properties with circumferential region following treatment with elastase (AL: n = 8; PL: n = 6; both median + IQR).

5.6.3.6 Effects of Degenerative Condition

Age and degenerative condition were found to be highly correlated ($r = 0.90$, $p = 0.002$). Independent assessment of age and degeneration dependencies was therefore not possible. As two of the three properties measured displayed no significant dependance on circumferential position (section 5.6.3.5) data from anterolateral and posterolateral specimens were pooled for this analysis.

Comparisons of pre-treatment results between specimens from non-degenerate and degenerate intervertebral discs are illustrated in Figure 5.23. Initial modulus and ultimate modulus were both found to be significantly greater for degenerate specimens ($p = 0.048$ and $= 0.005$ repectively). Extensibility was not found to be significantly different ($p = 0.549$)

Condition-related variations in mechanical properties following elastase treatment are illustrated in Figure 5.24, and following chondroitinase ABC treatment in Figure 5.25. No mechanical properties showed significant dependence on condition following either treatment (elastase: initial modulus, $p = 0.679$; ultimate modulus, $p = 0.090$; extensibility, $p = 0.805$; chondroitinase ABC: initial modulus, $p = 0.108$; extensibility, $p = 0.755$).

Condition-related variations in the magnitude of the changes in mechanical properties following elastase treatment are illustrated in Figure 5.26, and following chondroitinase ABC treatment in Figure 5.27. The magnitude of the changes showed no significant dependence on condition for either treatment (elastase: initial modulus, $p = 0.405$; ultimate modulus, $p = 0.785$; extensibility, $p = 0.805$; chondroitinase ABC: initial modulus, $p = 0.401$; extensibility, $p = 0.108$).

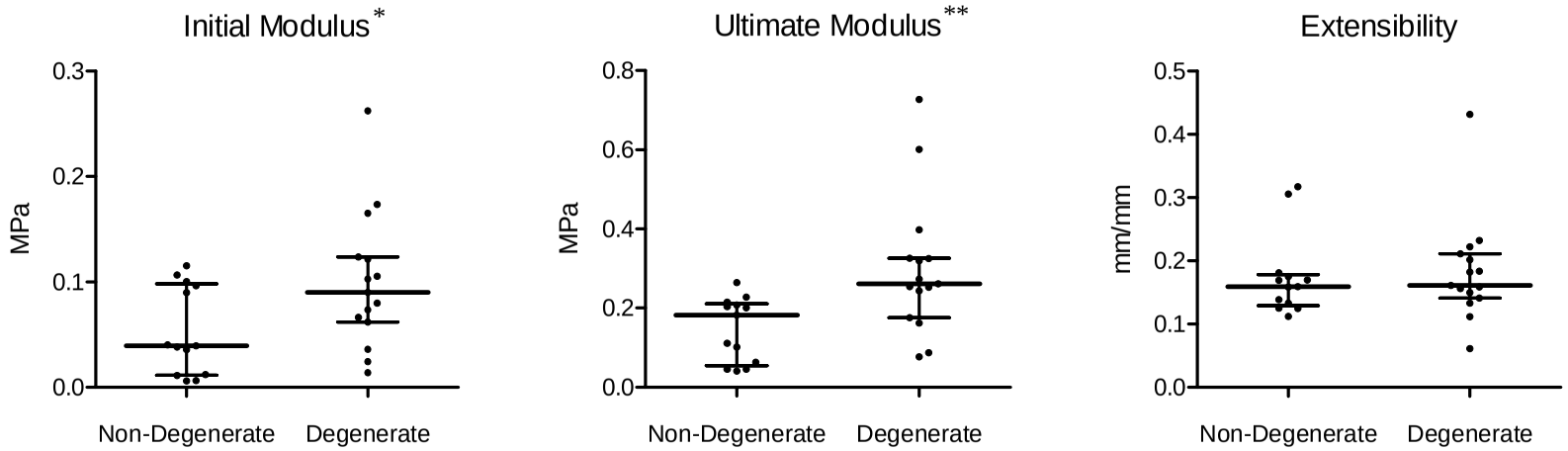


Figure 5.23. Variations in pre-treatment mechanical properties with disc condition (pooled anterolateral and posterolateral; non-degenerate: n = 13; degenerate: n = 15; all median + IQR). Significant difference between non-degenerate and degenerate, * p = 0.048, ** p = 0.005.

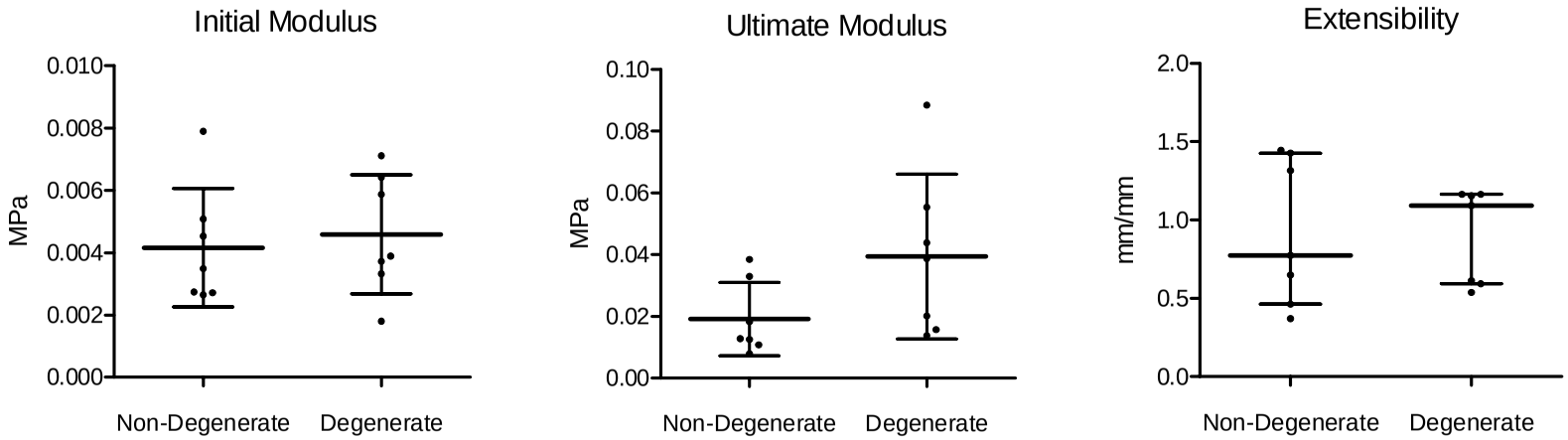


Figure 5.24. Variations in mechanical properties with disc condition following treatment with elastase (pooled anterolateral and posterolateral; non-degenerate: n = 7; degenerate: n = 7; initial modulus and ultimate modulus: mean ± SD; extensibility: median + IQR).

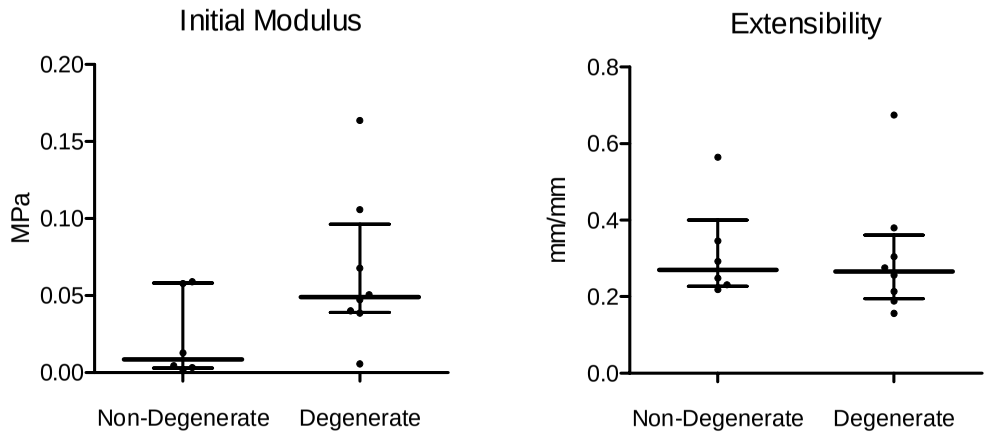


Figure 5.25. Variations in mechanical properties with disc condition following treatment with chondroitinase ABC (pooled anterolateral and posterolateral; non-degenerate: n = 6; degenerate: n = 8; both median + IQR).

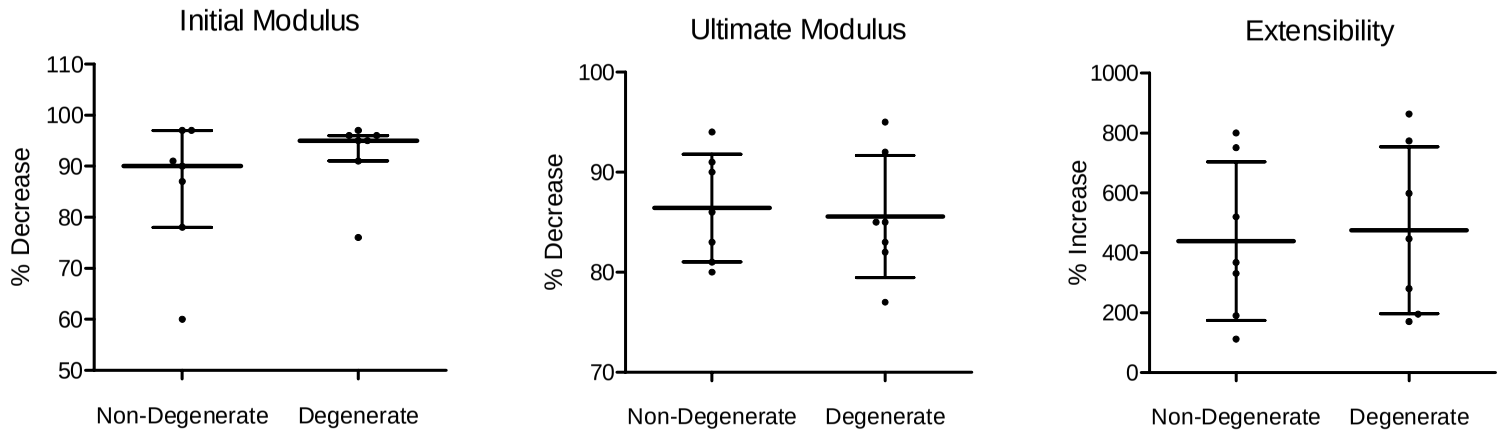


Figure 5.26. Variations in the magnitude of the changes associated with each of the mechanical properties with disc condition following treatment with elastase (pooled anterolateral and posterolateral; non-degenerate: n = 7; degenerate: n = 7; initial modulus: median + IQR; ultimate modulus and extensibility: mean ± SD).

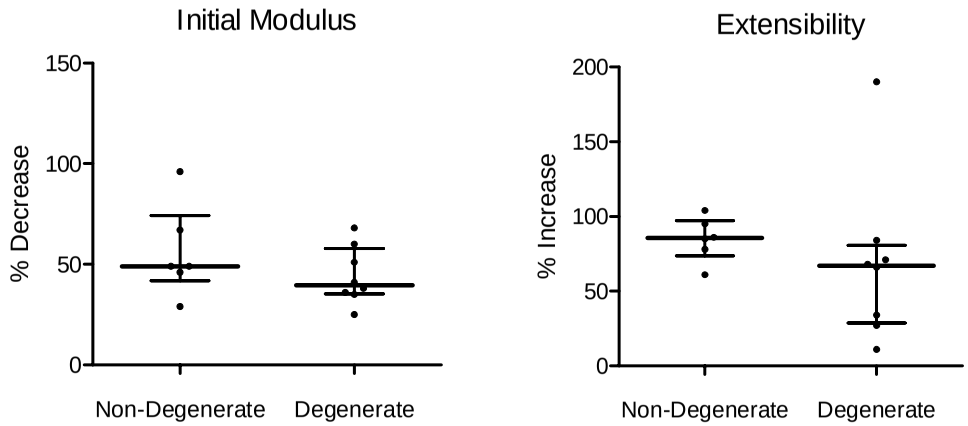


Figure 5.27. Variations in the magnitude of the changes associated with each of the mechanical properties with disc condition following treatment with chondroitinase ABC (pooled anterolateral and posterolateral; non-degenerate: n = 6; degenerate: n = 8; both median + IQR).

5.6.4 Discussion

In this chapter, the nature and magnitude of the contribution made by elastic fibres to the quasi-static tensile mechanical properties of the anulus in the radial direction was experimentally investigated using a combination of biochemically verified targeted enzymatic treatments and biomechanical tests.

Elastase treatment resulted in some unavoidable non-specific degradation of collagen despite the inclusion of soybean trypsin inhibitor. This small loss was considered unlikely to have confounded results both due to the significance of the observed changes in mechanical properties and the fact that specimens were tested perpendicular to the principle stress axes of the collagen fibres. Additionally, a previous study using similar techniques reported no effect on the mechanical properties of pure collagen, despite minor biochemical changes (Missirlis, 1977). The results presented in section 4.4.2 provide evidence that collagen microstructure is unaffected by enzymatic removal of elastic fibres.

As demonstrated by biochemical analyses, degradation of matrix components by enzymatic treatments was not absolute. Variability in the amount of elastin (measured as desmosine) was particularly high, making possible differences in results with both region and condition more difficult to elucidate.

Anulus mechanical properties in the radial orientation have been shown to be radially heterogeneous (Fujita *et al.*, 1997). The fact that radial position was not strictly controlled may have therefore contributed to the high variances associated with pretreatment mechanical properties. The strain rate that was used for the quasi-static ramp tests is comparatively high – as the anulus matrix comprises both solid

and fluid phases, a strain rate which exceeds the maximum flow rate of the fluid phase may somewhat exaggerate the initial modulus of the solid phase. This fact was considered unlikely to reflect on the validity of the results due to the comparative nature of the analyses. Additionally, there is evidence that the tensile response of radial specimens is not strain rate dependant (Fujita *et al.*, 1997).

The sample size of eight intervertebral discs was quite small, however the inclusion of repeated measurements within each disc, and the significance of the observed changes suggests that it was sufficiently powerful to satisfy the testing of the proposed hypotheses. It is possible that with slightly greater numbers, some trends observed in regional and condition comparisons may have become significant. The results presented in sections 5.6.3.5 and 5.6.3.6 should thus be treated as preliminary.

The repeatability of the mechanical testing protocol was tested in a preliminary study. None of the three mechanical properties measured showed a significant change between the initial and repeat test, indicating that neither the specimen mounting protocol nor the non-destructive quasi-static testing resulted in permanent tissue damage. It is possible that the semi-qualitative nature of the method used to define the maximum strain, in which particular care was taken not to exceed the yield strain of the tissue, may have resulted in slight underestimation of ultimate modulus, although the results of the repeatability study suggest the technique was effective.

Observed passive changes in specimen dimensions following respective enzyme treatments are consistent with the putative functional roles of elastic fibres and

glycosaminoglycans. Treatment with both elastase and chondroitinase ABC resulted in a significant decrease in cross-sectional area. This may reflect a decrease in glycosaminoglycans and the associated hydration, which normally accounts for a large percentage of the tissue volume. Following chondroitinase ABC treatment, specimen length decreased significantly, also consistent with a reduction in glycosaminoglycan and fluid volume. Following elastase treatment however, the opposite occurred, with length increasing significantly. This phenomenon appears consistent with the suggestion made in section 4.6 that elastic fibres may be under some initial pre-strain, and that in their absence the collagenous elements they interconnect undergo passive relaxation, and is also consistent with phenomena observed in other tissues where passive elongation of the tissue occurs following the removal of elastin (Lee *et al.*, 2001). It is noteworthy that this relaxation occurred to the extent that it more than compensated for any decrease associated with the accompanying loss of glycosaminoglycans.

Modulus values determined in this study compare favourably with those determined previously for radially oriented specimens, with any differences likely attributable to dissimilarities in specimen preparation techniques, and whether dimensions were measured before or after saline equilibration (Marchand and Ahmed, 1989; Fujita *et al.*, 1997; Elliott and Setton, 2001). Importantly, modulus values are also comparable to those determined for single lamellar, circumferential plane specimens tested perpendicular to the collagen fibre direction (Holzapfel *et al.*, 2004).

In general, all three mechanical properties displayed high inter-specimen variability, likely due to the extensive localised structural heterogenity of the anulus matrix. For example, previous observations that deformation transverse to the lamellae occurs

by way of both bundle elongation and lamellar separation (Pezowicz *et al.*, 2006a), suggest that intralamellar and interlamellar mechanical properties are unique. The mechanical properties measured in this study may therefore be dependant on both the number of lamella present within the gauge region and the number of collagen bundles within each of those lamellae. This structure-function association could be investigated further in future studies.

Following treatment with elastase, specimens exhibited large and significant reductions in initial and ultimate modulus, and increases in extensibility. These results enable rejection of each of the null hypotheses proposed at the chapter outset. They suggest that elastic fibres function to guide and restrain the deformation of the collagen matrix, and that on their removal, collagenous elements are able to separate and rearrange more easily and to a greater extent. Following treatment with chondroitinase ABC, specimens exhibited significant, although much more moderate respective reductions in initial modulus and increases in extensibility, and no significant change in ultimate modulus.

Given that experimental results demonstrate that elastic fibres contribute significantly to both the initial toe region and second linear regions of the stress-strain response, it is useful to consider, conceptually, the structural mechanisms underlying those contributions. As elastic fibres in isolation exhibit highly linear behaviour (section 1.2.2.2), a contribution in the toe region suggests some initial alignment of elastic fibres, and those collagenous elements which they interconnect, towards the loading direction. This toe region contribution may well be exaggerated by the testing direction – applying radial strains means that the majority of fibrous elements are initially transverse to the loading direction. Were strains to be applied

to specimens progressively oriented closer to the collagen fibre bundle direction, it is conceivable that the toe region contribution of elastic fibres would decrease. It is noteworthy that the median ultimate modulus for untreated specimens is of the same order of magnitude of pure elastin (Fung, 1981).

Extensibilities of untreated specimens were generally greater than the mean radial tensile strains that occur in the anulus during physiological loading, which range from 4.7 percent to 9.8 percent depending on circumferential position, degenerative condition and loading modality (Tsantrizos *et al.*, 2005), indicating that physiological radial strains occur predominantly within the initial toe region of the response. Extensibility was found to be significantly greater for posterolateral specimens than for anterolateral specimens, both before and after elastase treatment. This difference may be partially attributable to heterogeneity in the collagenous architecture, which has been demonstrated to be of greater complexity in the posterolateral region (Tsuji *et al.*, 1993). This represents an important, and until now unreported structure-function association, which may reflect the greater and more complex physiological stresses and strains experienced by this region of the anulus (Edwards *et al.*, 2001; Schmidt *et al.*, 2007). In Chapter 3, intralamellar elastic fibre density was found to be greater in this region of the anulus, possibly enabling the matrix to recover from larger and more complex deformations. This may represent a mechanobiological or evolutionary response designed to enhance the mechanical integrity in this region, a common site for radial fissures leading to nuclear prolapse (Haefeli *et al.*, 2006).

The tensile mechanical properties of the anulus fibrosus at the tissue level have been shown previously to exhibit dependance on degenerative condition: in the

circumferential orientation Poisson's ratio, failure stress, strain energy density and elastic modulus are all influenced by degeneration (Acaroglu *et al.*, 1995). The results of this study extend these findings to the radial orientation, demonstrating that both initial modulus and ultimate modulus are higher for degenerate specimens. Physiologically, both radial and circumferental strain magnitudes are greater for degenerate specimens (Tsantrizos *et al.*, 2005). A consequence of higher physiological strains combined with a stiffer matrix may be the increased likelihood of mechanical damage manifested as matrix cracking and delamination, both of which are common artifacts observed macroscopically in the degenerate anulus (Iatridis and ap Gwynn, 2004). It is possible that these changes occur as a consequence of spatial changes in stress distribution that occur with degeneration (Adams *et al.*, 1996). The elastin content of the anulus has recently been shown to increase with degeneration, possibly representing a functional response designed to reinforce collagen matrix cohesion in response to such changes in stress distribution (Cloyd and Elliott, 2007). As suggested previously, further studies are required to determine whether this increase in elastin occurs within collagen bundles, at lamellar interfaces or both. An increase in elastin as a primary source of increasing stiffness with degeneration would potentially be exaggerated by an accompanying decrease in hydration, as without exposure to adequate hyrdation, elastin loses its rubber like elasticity, ultimately approaching a brittle glass point (Kakivaya and Hoeve, 1975; Gosline, 1976).

While previous studies have used enzymatic degradation to demonstrate important relationships between glycosaminoglycan content and compressive modulus and permeability, this study is the first to demonstrate that the tensile role of

glycosaminoglycans is also significant, specifically with respect to initial modulus and extensibility (Perie *et al.*, 2006a; Perie *et al.*, 2006b). This suggests that an age related decrease in glycosaminoglycan content may reduce the shock-absorbing capacity of the anulus matrix in tension. The role of glycosaminoglycans appears to be distinct in nature and magnitude from that of elastic fibres, which were found to enhance initial elastic modulus and extensibility to a greater extent, as well as maintain the mechanical integrity of the collagen matrix at higher relative stresses.

Mechanical testing results, in combination with the results of the histological studies described in Chapters 3 and 4, suggest that any loss of elastic fibres with age or pathology may reduce the transverse integrity of collagen fibre bundles, possibly enhancing the ability of radial lesions to propogate through lamellae, and weaken interlamellar cohesion, possibly contributing to the formation of circumferential tears. Alternatively, results suggest that any increase in elastic fibre density with age may represent a functional adaption by the anulus matrix to repetitive loading. It is clear that further studies are required to determine the nature and extent of any such variations.

While in this investigation radially oriented specimens were studied, the results as they pertain to the functional role of elastic fibres may be equally applicable to any specimen orientation where deformation occurs by way of transverse separation and rearrangement of collagenous elements. The fact that quasi-static properties of specimens oriented parallel to the circumferential surface of the disc and tested perpendicular to the collagen bundle direction are comparable to those determined in this study supports this theory (Holzapfel *et al.*, 2004) .

Finally, these results provide the basis for the development of new and improved material models to accurately describe the mechanical behaviour of the intervertebral disc in terms of the individual contributions of its extracellular constituents. A model was recently proposed for the anulus fibrosus which included terms representing the contributions of collagen fibres, extrafibrillar ground matrix, and fibre-matrix interactions provided by non-collagenous consituents (Guerin and Elliott, 2007). This model predicted that normal and shear interactions regulated by these constituents contribute significantly to multi-dimensional anulus fibrosus mechanical behaviour. The results presented here provide experimental evidence of the nature and extent of that contribution, and identify elastic fibres as a major interactive structural candidate.

CHAPTER 6: SUMMARY AND FUTURE WORK

Descriptions of structure-function relationships within the extracellular matrix of soft biological tissues such as the anulus fibrosus are important for several reasons: they enable researchers to understand, model and predict mechanical damage; they highlight potential therapeutic targets for slowing or reversing the degenerative process; they aid efforts to successfully engineer functionally accurate synthetic and biological tissue replacements. The overall objective of this thesis was to expand current understanding of the structural and functional roles played by elastic fibres in the anulus fibrosus of the human lumbar intervertebral disc.

In Chapter 3, the development of novel imaging techniques enabled elastic fibres in the anulus fibrosus to be visualised at a level of detail not previously achieved. Comparisons of elastic fibre arrangement between the intralamellar and interlamellar regions revealed differences which suggested that elastic fibres perform functional roles at these two distinct levels of the collagen structural hierarchy. Within collagen bundles, the arrangement of elastic fibres was observed to be predominantly parallel to the direction of the collagen fibres, however the degree of isotropy appeared to vary with both radial and circumferential position. At the interfaces between consecutive lamellae, elastic fibres were observed to form multidimensional meshworks that connected adjacent collagen bundles with opposing fibre directions. A quantitative investigation revealed that the density of elastic fibres within lamellae was radially and circumferentially heterogeneous. Density was greater in outer regions than in inner regions, and greater in posterolateral regions than in anterolateral regions. It was suggested that these variations may reflect the magnitude of the tensile deformations experienced by the anulus fibrosus physiologically in bending and torsion.

In Chapter 4, the nature of the structure-function associations between elastic fibres and collagen was investigated with respect to the distinct structural mechanisms that are known to facilitate tensile deformation of the collagen matrix. Enzymatic removal of elastic fibres had no observable effect on the passive behaviour of collagen fibre planar crimp, suggesting that a minimal role is played by elastic fibres maintaining and re-establishing this crimp. In specimens subjected to radial tensile strains, reorientation of collageneous elements was observed to result in multiple patterns of rearrangement with respect to elastic fibres, including loss of isotropy, crumpling and extension, in addition to multiple structural transformations with respect to individual fibres. Additionally, bundles of elastic fibres were observed to maintain physical connections between consecutive lamellae undergoing localised transverse separation. These observations suggested that elastic fibres provide important mechanical cross-connectivity, both within lamellae between adjacent collagen fibres, and between consecutive lamellae.

In Chapter 5, the nature and magnitude of the contribution made by elastic fibres to the tissue-level mechanical properties of anulus fibrosus was investigated. Biochemically validated enzymatic treatments were developed which allowed selective degradation of elastic fibres and glycosaminoglycans from the anulus matrix. Uniaxial quasi-static tests were applied to radially oriented specimens allowing direct assessment of the role played by elastic fibres in enhancing the transverse mechanical integrity of the collagen matrix both within and between lamellae. Results demonstrated that in the absence of elastic fibres, mechanical integrity was weakened, characterised by significant reductions in initial modulus and ultimate modulus, and increases in extensibility. These results suggest that any

pathological or chronological decrease in elastic fibres would weaken the mechanical integrity of the anulus at each level of the structural hierarchy, promoting the formation of degenerative features such as radial fissures and circumferential tears. Alternatively, they suggest that an increase in elastic fibres may represent a mechanobiological reaction designed to reinforce the matrix following mechanical fatigue.

There are currently contradictions in the literature regarding the nature of the changes to the anulus fibrosus elastic fibre network that occur with aging and degeneration. Early studies suggested that fibre content peaks at maturation, then declines (Johnson *et al.*, 1985; Olczyk, 1994); however a more recent study showed a strong positive correlation between elastin content and degree of degeneration (Cloyd and Elliott, 2007). Given the importance of elastic fibres for mechanical function as demonstrated in this thesis, clarification of the nature of the changes in elastic fibre distribution and density with age and pathology is critical. Such studies could be either histological or biochemical, but should be conducted in the context of the significant structural heterogeneity in the elastic fibre network which has been described. In the context of these potential changes, irrespective of their nature, biological investigations examining the presence and distribution of elastic fibre degrading proteases and matrix metalloproteinases relative to their respective tissue inhibitors are also potentially very important. An example of such an investigation would be to compare the relative genetic expressions of these enzymes in intervertebral discs at various ages and stages of degeneration.

The mechanical investigation in this thesis was limited to examining the contribution of elastic fibres at the tissue level. Future studies should address this

contribution at the motion segment level. The application of the enzymatic degradation techniques descibed here may be problematic for studying motion segments, as the ability to ensure uniform diffusion of the enzyme over such a large area would be difficult, however they may be applicable for well-established small animal models, such as rats. Alternatively, elastin or fibrillin knock-down and knock-in animal models may potentially be valuable future tools for such studies.

In this thesis, the mechanical testing orientation (radial) was selected to most directly test the nature and magnitude of the contribution made by elastic fibres to cross-collagen fibre and cross-lamellar connectivity. Future studies should expand on these results to include other test orientations and other structure-function associations. For example, results suggest that elastic fibre degradation impacts significantly on the mechanisms which underly collagen fibre reorientation in axial and circumferential expansion – studies could therefore investigate potential correlations between elastic fibre density and changes to collagen fibre tilt angle, and examine the effect of targeted enzymatic removal of elastic fibres on that property. The enzymatic techniques developed in Chapter 5 could also potentially provide a useful tool for experimentally validating current and future structure-function analytical models of anulus fibrosus behaviour.

The investigations described in this thesis were limited to uniaxial tests. In reality, the physiological behaviour of the motion segment subjects the anulus to complex biaxial strains; biaxial tests could therefore add an important additional layer of sophistication to the results presented, and complement further multidirectional unaxial tests.

Tissue engineering is potentially a very important tool for the repair and replacement of degenerate intervertebral discs (O'Halloran and Pandit, 2007). Studies to date have focussed on the successful synthesis of proteoglycans and collagen by anulus fibrosus and nucleus pulposus cells seeded on scaffolds, as those constitutents which are required to achieve in-vivo structural and functional equivalence (Mizuno *et al.*, 2006; Wilda and Gough, 2006; Nerurkar *et al.*, 2007). In light of the findings presented in this thesis, in the future such studies should be expanded to investigate and promote the production and integration of elastic fibres. It is likely that inclusion of elastic fibres which transversely integrate collagenous elements would enhance the ability of tissue engineered structures to replicate the mechanical anisotropy of the anulus matrix. Organ culture systems of the kind used in tissue engineering also present the opportunity to investigate the types of mechanical stimuli which result in the production of elastic fibres and their distribution in the patterns described at each level of the anulus structural hierarchy.

In summary, the findings presented in this thesis provide important new insights into the structure and mechanical function of the anulus fibrosus elastic fibre network. Additionally, the techniques which have been developed present a substantial and robust platform for future experimental structure-function investigations, both with respect to the intervertebral disc and other soft biological tissues.